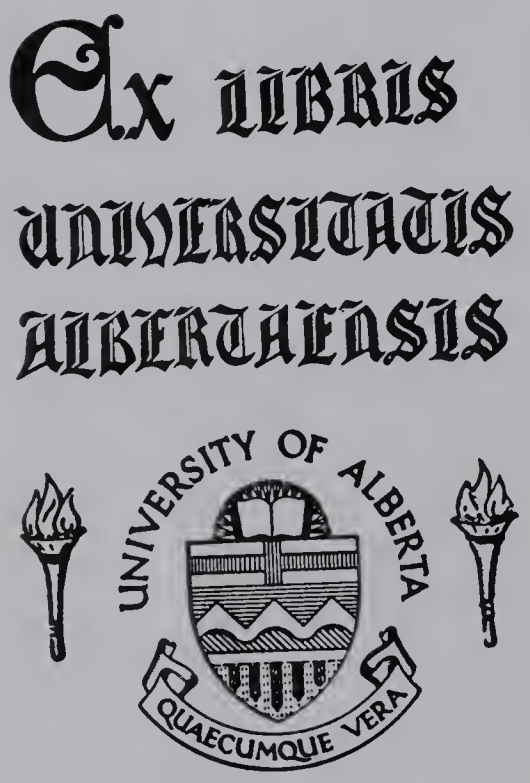

University of Alberta
Printing Department

THE UNIVERSITY OF ALBERTA

ROTATION CAPACITY OF WIDE-FLANGE BEAMS UNDER MOMENT GRADIENT

by

ALBERT FRANKLIN LUKEY

A THESIS

SUBMITTED TO THE FACULTY OF GRADUATE STUDIES

IN PARTIAL FULFILMENT OF THE REQUIREMENTS FOR THE DEGREE OF

MASTER OF SCIENCE

DEPARTMENT OF CIVIL ENGINEERING

EDMONTON, ALBERTA

MAY, 1967

UNIVERSITY OF ALBERTA

FACULTY OF GRADUATE STUDIES

The undersigned certify that they have read, and recommend to the Faculty of Graduate Studies for acceptance, a thesis entitled ROTATION CAPACITY OF WIDE-FLANGE BEAMS UNDER MOMENT GRADIENT submitted by ALBERT FRANKLIN LUKEY in partial fulfilment of the requirements for the degree of Master of Science.

ABSTRACT

This investigation attempts to relate the flange slenderness ratio to the rotation capacity of steel wide-flange beams subjected to a moment gradient.

The results of twelve tests are reported. The tests were performed on simply-supported beams of CSA G40.12 steel, subjected to a concentrated load at midspan. The flange and web geometry were varied, while the laterally unbraced slenderness ratio was held constant. All tests were continued until substantial unloading had occurred due to the effects of instability.

The plastic hinge rotations delivered by the present test specimens and others are compared to the maximum practical requirements for plastically designed continuous beams. For short beams, it is shown that the requirements can be met by very slender-flanged sections. It is concluded, however, that the available experimental evidence is insufficient to allow firm conclusions to be drawn regarding the allowable flange slenderness ratios for long beams having low moment gradients.

A series of tests is proposed to further define the effects on rotation capacity of varying the moment gradient and the lateral bracing spacing.

ACKNOWLEDGEMENTS

This study is part of a continuing investigation "Local Buckling of High Strength Steel Members" currently being carried out at the Department of Civil Engineering, University of Alberta. Professor P.F. Adams is the Project Director. The project is sponsored financially by the Canadian Steel Industries Construction Council, with technical assistance from the Canadian Institute of Steel Construction.

The assistance of Mr. G.T. Trotter, Alberta Regional Engineer, C.I.S.C.; Mr. J.C. Taylor, Chairman, Engineering and Research Sub-Committee of the Alberta Regional Committee, C.I.S.C.; and Mr. H.A. Krentz, Assistant Chief Engineer, C.I.S.C., is particularly acknowledged.

The author wishes to express his sincere appreciation to Professor P.F. Adams under whose direction the work was performed and whose advice and continuing guidance were most valuable.

The comments and criticisms of Professor J. Longworth and J.S. Kennedy, who served on the thesis committee, are gratefully acknowledged.

The contributions of Mr. H. Panse and members of the laboratory staff in carrying out the testing program, and Miss H. Wozniuk, who typed the report, are also acknowledged gratefully.

TABLE OF CONTENTS

LIST OF TABLES

LIST OF FIGURES

LIST OF FIGURES (continued)

CHAPTER I

INTRODUCTION

The allowable stress methods of structural design[1,2] limit the working loads so that the computed elastic stresses do not exceed prescribed values, taken as some proportion of the nominal yield stress. Tacit recognition is given to inelastic structural action in some cases, usually be increasing the allowable stresses[1,2]. However, no attempt is made to specify the ultimate load capacity of the structure.

The plastic design methods, on the other hand, attempt to predict the actual collapse load for the structure by explicitly considering the ductile properties of the material. The design collapse loads are determined by multiplying the working loads by appropriate load factors.

FIGURE 1.1 shows the initial portion of an idealized stress-strain (σ - ϵ) curve for structural steel in either tension or compression. For strains below the yield strain, ϵ_y , the material is elastic, with the slope of the stress-strain curve defined as the elastic modulus, E . As the strain is increased beyond ϵ_y , the stress remains constant at the yield stress, σ_y , up to a strain of ϵ_{st} , which represents the onset of strain-hardening. At this point the stress again begins to increase with increasing strain. The slope of the curve in this range is E_{st} , the strain-hardening modulus.

In "simple plastic" theory it is assumed that all elements of

a given cross-section in a member subjected to flexure remain elastic up to the attainment of the "plastic moment", M_p, which is the moment corresponding to a stress of $\pm \sigma_y$ in all elements of the section. It is further assumed that, once the plastic moment has been reached, the moment at that cross-section remains at the plastic moment value for all further increases in strain. Applied to a redundant structure, this means that the first cross-sections to reach the plastic moment will continue to rotate at that moment value until sufficient sections have yielded to produce an unstable linkage or "mechanism". Such plastically rotating sections are known as "plastic hinges".

This assumed behavior conservatively neglects the additional moment capacity due to the effects of strain-hardening. However, it also ignores the possibility that the moment capacity at a plastic hinge may be reduced by instability phenomena at a rotation smaller than that required to form a mechanism.

FIGURE 1.2 shows a plot of moment, M , non-dimensionalized as M/M_p, vs. rotation for a simply-supported wide-flange beam. The length of the beam is 2L and it is subjected to a concentrated load, P , at mid-span. $\theta/2$ denotes the change of slope at each support. $\theta_p = M_p L/EI$ denotes the total of the two end rotations which would correspond to a moment, M_p, at midspan if the beam were to remain completely elastic. The dashed curve represents the behavior assumed in simple plastic theory. The solid curve, showing actual behavior, departs from the idealized curve at first yielding. Above this yield load, rotation occurs at an

increasing rate due to the penetration of yielding through the cross-section and the spread of the yielded zone along the length of the beam from the point of maximum moment. M_p is reached and exceeded due to strain-hardening of the outer fibers. Finally, local buckling occurs within the yielded portion of the compression flange and this precipitates a drop-off in moment capacity. This behavior is typical of beams subjected to loads producing moments which vary along the length of the member (moment gradient). The "rotation capacity" of the beam has been defined[3] as $R = \theta/\theta_p - 1$, where θ is the rotation at which M drops below M_p. The absolute inelastic hinge rotation, $\theta - \theta_p$, of the full span will be denoted by the term "hinge capacity".

The actual hinge capacity of a member in a given structure must exceed the hinge rotation required to form a mechanism in order to insure that the ultimate load of the structure will reach or exceed that predicted by simple plastic theory. The factors which limit hinge capacity are, therefore, of concern, and they can best be studied by considering the following two basic situations involving post-elastic buckling of beams:

(a) regions of constant moment, where unloading is usually brought about by lateral deflection of the compression flange, which precipitates local buckling, and

(b) regions of moment gradient, where unloading is usually initialized by local buckling of the compression flange with subsequent lateral buckling of the unbraced span.

Beams subjected to uniform moment have been investigated extensively[3,4,5,6] and will not be further explored herein. The case of beams under moment gradient has received some recent analytical study[7,8] and a limited amount of experimental study[6,9,10]. However, the results to date have not sufficiently defined the effects of flange and web geometry on the hinge capacity, particularly for high strength steel members.

Because beams subjected to moment gradient are most commonly encountered in structural practice, there is a definite need for more experimental study in this area. The present investigation was undertaken to attempt to relate the flange slenderness ratio, b/t , to the hinge capacity of high strength steel beams.

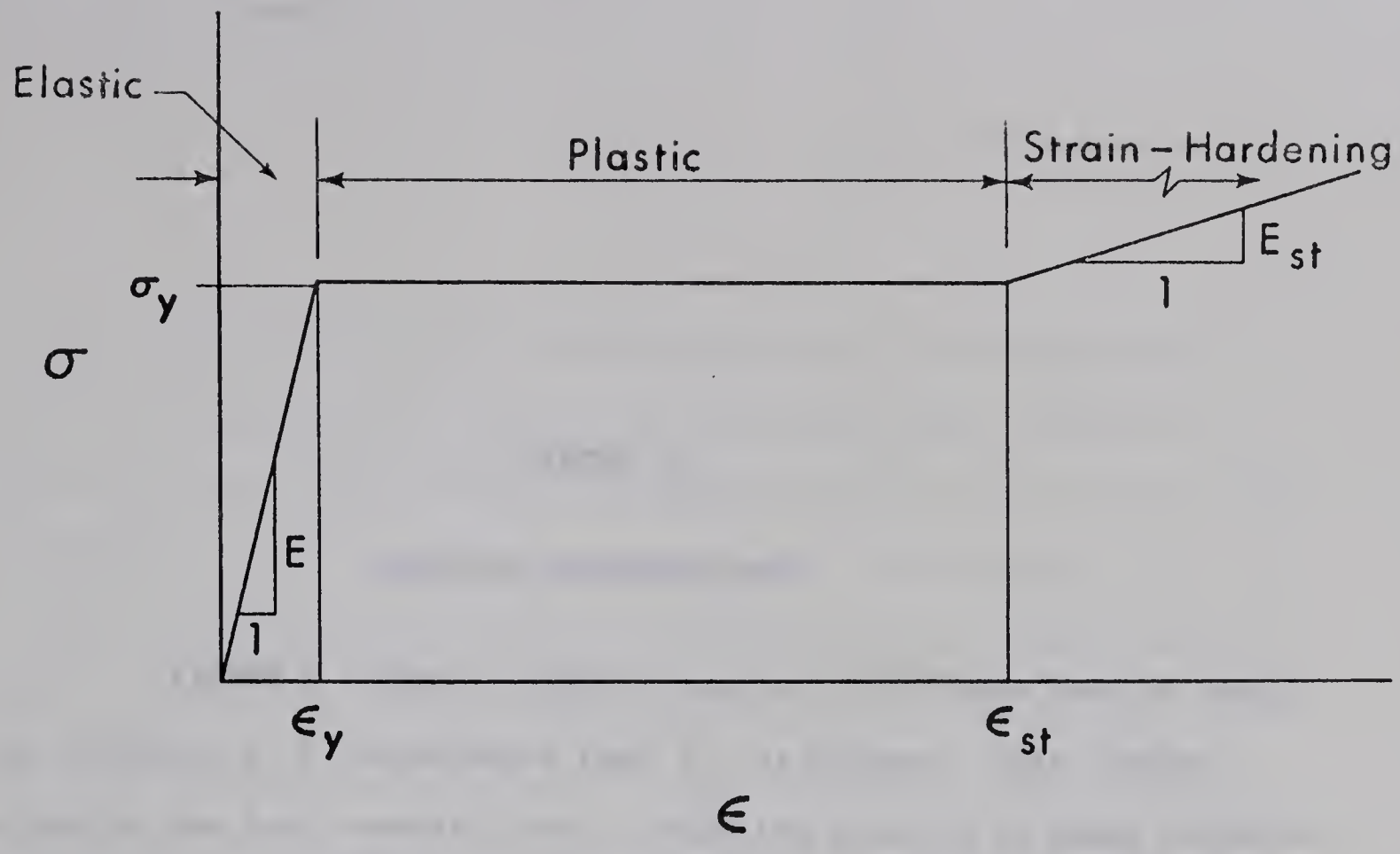

FIGURE 1.1 STRESS-STRAIN RELATIONSHIP

FIGURE 1.2 MOMENT-ROTATION RELATIONSHIP

CHAPTER II

PREVIOUS INVESTIGATIONS

FIGURE 2.1 shows a simply supported wide-flange beam of length 2L, subjected to a concentrated load, P , at midspan. This loading situation has been commonly used to study the behavior of beams subjected to moment gradient[6,10].

The applied load, P , is of a magnitude such that the midspan moment, $M_o = PL/2$, exceeds the moment, M_{ps} , required to cause yielding of the flanges. Between the points at which the moment equals M_{ps} , the flange is in a fully yielded state. This total yielded length is represented by $2\tau L$ in FIGURE 2.1(b), where τ is the proportion of length yielded. If M_{ps} is approximated by M_p[7] the curvature diagram corresponding to this moment configuration is as shown in FIGURE 2.1(c). This assumes the material properties given in FIGURE 1.1 and a shape factor, f , of 1.0, where $f = M_p/M_y$, and M_y denotes the moment at first yielding. $\phi_p = M_p/EI$ is the curvature corresponding to the attainment of M_p , assuming an ideally elastic material, while s represents the ratio of the curvature at the onset of strain-hardening to ϕ_p . The curvature jumps from ϕ_p to $s\phi_p$ at a moment of M_p , and continues to increase with increasing moment to the value shown at midspan. In this expression, $h = E/E_{st}$. For the structural steels the plastic hinge rotation can be approximated by the cross-hatched area in FIGURE 2.1(c)[7].

Lay and Galambos[8] have recently carried out an analytical study of the post-elastic behavior of wide-flange beams subjected to moment gradient. The lateral buckling model used in this study is shown in FIGURE 2.2. It consists of a column composed of the compression tee laterally unbraced over a length, L , and subjected to a uniform axial load, σ_y A/2. The yielded length of the column is τL , and the rotational restraint provided by the adjacent span at the elastic end is represented by the spring constant S EI_{yy}/L. The lateral buckling solution based on this model is taken to represent a lower bound for beams of practical structural proportions. A graphical representation of the solution for members of A36 steel is given by the solid curves plotted on FIGURE 2.3 for various values of the end restraint factor, S . The ordinate in FIGURE 2.3 is the proportion of length yielded, τ , and the abscissa is the slenderness factor

$$\lambda = \frac{L}{r_y} \left(\frac{\sqrt{\epsilon_y}}{\P}\right)$$

where r_y is the weak axis radius of gyration.

The dashed curves plotted in FIGURE 2.3 represent the local buckling solution[8] which will be described below. A comparison of the solid and dashed curves indicates that local buckling will occur at a shorter yielded length than will lateral buckling for all values of λ below about 0.7, even though the lateral buckling curves represent a lower bound solution. Thus, it is concluded that, for most practical

beams under moment gradient, failure will be triggered by local buckling. The present test series involves beams having values of the slenderness factor, λ , in the order of 0.5. Therefore, theoretical work dealing with local buckling is of primary importance to this study.

Haaijer and Thurlimann[9] applied the energy method to the buckling of a uniformly compressed plate. The case related to flange buckling was that of a rectangular plate simply supported at the two loaded (transverse) edges, free on one longitudinal edge, and elastically restrained at the other. Because the post-elastic buckling of beams involves deformations in the strain-hardening range, it was necessary to evaluate the material properties under these conditions. These were determined experimentally from tests on specimens of A7 steel. Since the theory considered the orthogonal anisotropy of the material, it was necessary to determine five different material stiffnesses as well as the coefficient of web restraint.

Due to the empirical manner of evaluating the material constants, Haaijer's results are not directly applicable to steels other than A7.

Lay[7] used the model shown in FIGURE 2.4(a) to analyze flange local buckling in a beam subjected to moment gradient. The model consists of a fully yielded length of plate, L , of width, b and thickness, t , subjected to a uniform axial compressive stress, σ_y . The restraint of the web is represented by a torsional spring of stiffness, k_ϕ . The torsional buckling equation for this case is given by[7,11].

$$P = \frac{1}{r_o^2}\left[G_{st}K_T + \left(\frac{n\P}{L}\right)^2 E_{st}I_w + k_\phi\left(\frac{L}{n\P}\right)^2\right] \tag{2.1}$$

in which $P = \sigma bt$, and L/n represents the half wavelength of the local buckle. K_T and I_w are the St. Venant torsional constant and the warping constant respectively and are properties of the cross-section. The value of k_ϕ, determined by considering the two-dimensional model of web deformation shown in FIGURE 2.4(b), is given as[7]

$$k_\phi = \frac{G_{st}w^3}{3(d - 2t)} \tag{2.2}$$

The material constants, E_{st} and G_{st} are the extensional and torsional moduli, respectively, in the strain-hardening range. G_{st} is given by:

$$G_{st} = \frac{2G}{1 + \frac{h}{4(1 + \mu)}} \tag{2.3}$$

where G is the elastic shear modulus and μ is Poisson's ratio in the elastic range. By assuming the number of half wavelengths, n, to be a continuous function, equation (2.1) can be differentiated with respect to (n/L) to determine the wavelength corresponding to a minimum value of P. Substitution of this L/n value back into equation (2.1) then yields the load, P, at which buckling will occur. Conversely, assuming P to

$$\frac{}{}$$

be the yield load, $\sigma_y bt$, or some other value, the critical section properties may be determined for given material properties.

FIGURE 2.5 indicates the length of flange, τL , which must be yielded in order for local buckling to occur. The shape of the local buckle is assumed to be completely restrained at the load or reaction point at one end and by the relatively stiff elastic portion at the other, so that the yielded length must equal or exceed one full wavelength, as calculated from Equation (2.1), in order for a local buckle to form at a minimum stress.

Lay has assumed, for the case of a beam under moment gradient, that the maximum average stress over the required yielded length of compression flange is

$$\sigma_y^* = \frac{1}{4} \left(3 + \frac{\sigma_u}{\sigma_y}\right) \sigma_y \qquad (2.4)$$

where σ_u is the ultimate stress. This is taken to represent a conservatively high estimate of the average stress in the yielded zone[8]. Using this stress value, the critical flange slenderness (b/t) can be computed. Further, assuming that the web restraint effects an average increase of 2.6% in the allowable b/t ratio, the following equation for critical flange slenderness is obtained[7]:

$$(b/t)^2 = \frac{12.64}{3 + \frac{\sigma_u}{\sigma_y}} \cdot \frac{1}{\epsilon_y} \cdot \frac{1}{1 + \frac{h}{5.2}} \qquad (2.5)$$

The value of h used corresponds to the initial slope of the strain-hardening curve. Equation (2.5) then yields a critical b/t ratio almost identical to the present A.I.S.C. code requirement for compact sections[2].

A completely different approach has been proposed by Kato[12], who used a modified yield line theory to compute the ultimate strength of the flange plate. However, this approach has not yet been developed into a useable form.

Experimental work on local buckling of wide-flange beams in the strain-hardening range was reported by Haaijer and Thurlimann in 1954[9]. Six stub columns and six beams under uniform moment were tested, all of A7 steel. The strains at which local buckling occurred were measured for all specimens tested. The results are summarized in FIGURE 2.6, which plots critical strain, ϵ_{cr}, versus flange slenderness, b/t. The beam and stub column tests are differentiated by plotting them as circles and squares, respectively. The strain, ϵ_{st}, at the onset of strain-hardening for A7 steel is shown as the horizontal dashed line.

By assuming that sufficient plastic rotation would occur in a beam if its flange strains reached ϵ_{st} before the occurrence of local buckling, it was concluded that the critical b/t ratio for wide-flange beams of A7 steel was 17. This conclusion was based primarily on the stub column tests. As can be seen from FIGURE 2.6, the beam tests would indicate a critical b/t somewhat higher than 17. The results of these tests form the basis for the present (1967) A.I.S.C.[2] and C.S.A.[1] code limitations for plastically designed beams, both under uniform

moment and under moment gradient.

Sawyer[10], in 1961, reported the results of 21 tests on simply-supported wide-flange beams subjected to a concentrated load at midspan. The steel used had flange yield stresses ranging from 38 ksi to 44 ksi, as determined from tension tests performed at a strain rate approximately twice the maximum allowed by A.S.T.M.[13]. Rolled sections having flange slenderness ratios from 10.7 to 18.7 were tested. All but three of the specimens were braced laterally at the load point and at the supports. Eleven of the specimens were deformed into the unloading range, while the remainder of the tests were terminated at the attainment of maximum load. The strain rate used was not defined in the inelastic range, which has raised some question as to the interpretation of the results[14].

Adams, Lay and Galambos[6], in 1965, reported the results of a series of tests performed on A441 steel wide-flange members having a nominal yield stress of 50 ksi. This series included three simply supported beams under moment gradient which were deformed well into the unloading range. However, the only significant geometric parameter to be varied in the tests was the unbraced slenderness ratio, L/r_y. Thus, the tests produced little information regarding the effects of flange and web slenderness on rotation capacity.

In order to determine whether the delivered hinge capacity of a given member is adequate it is first necessary to know the hinge capacity required to form a mechanism in a particular structural situation. Analytical studies have been performed to determine maximum plastic

rotation requirements for practical structures.

Kerfoot[15] has analyzed the symmetrical 3-span beam subjected to point loadings shown in FIGURE 2.7. The length ratio, α , and the load ratio, β , were varied in this study to provide a range of situations in which plastic hinge rotations were required both in regions of constant moment and of moment gradient. This study indicated that, only for very extreme values of α and β would the required hinge capacity at any point exceed $\phi_p L$, where $\phi_p = M_p/EI$ and L is shown in FIGURE 2.7.

An analysis of frames[4,16] has indicated that the largest required plastic hinge rotation for a single span rigid frame such as that shown in FIGURE 2.8 is $1.03\ \phi_p L$. In more complex structures the theoretical hinge angle required to form a mechanism may be rather large[16]. However, it has been shown that, for such structures, a load close to the ultimate can be attained with much smaller hinge rotations. This is illustrated in FIGURE 2.9, taken from Reference 17. The load, P , non-dimensionalized as P/P_u , is plotted against the plastic rotation, θ_H , of the first hinge to form, represented non-dimensionally as $\theta_H EI/M_p L$. The structure considered is the two-span portal frame shown in the inset. The hinge angle at formation of a mechanism is $1.52\ M_p L/EI$, but 98% of the ultimate load is reached at a rotation of $0.54\ M_p L/EI$. Since the attainment of 98% of the calculated ultimate load would be considered satisfactory for design purposes, it is concluded that practical rotation capacity requirements need not be related to the large theoretical rotations encountered in highly redundant frames[17].

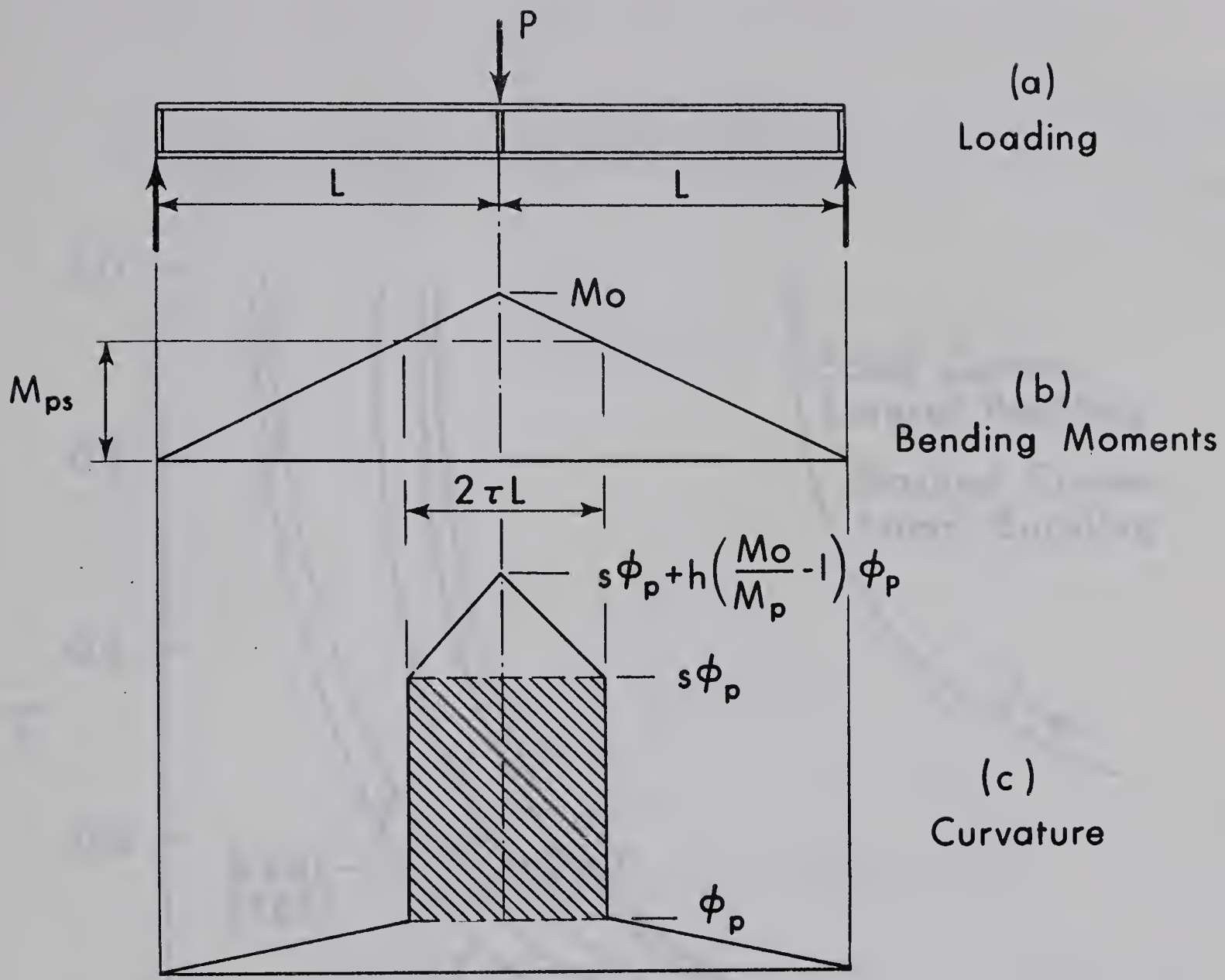

FIGURE 2.1 SIMPLY SUPPORTED WIDE-FLANGE BEAM

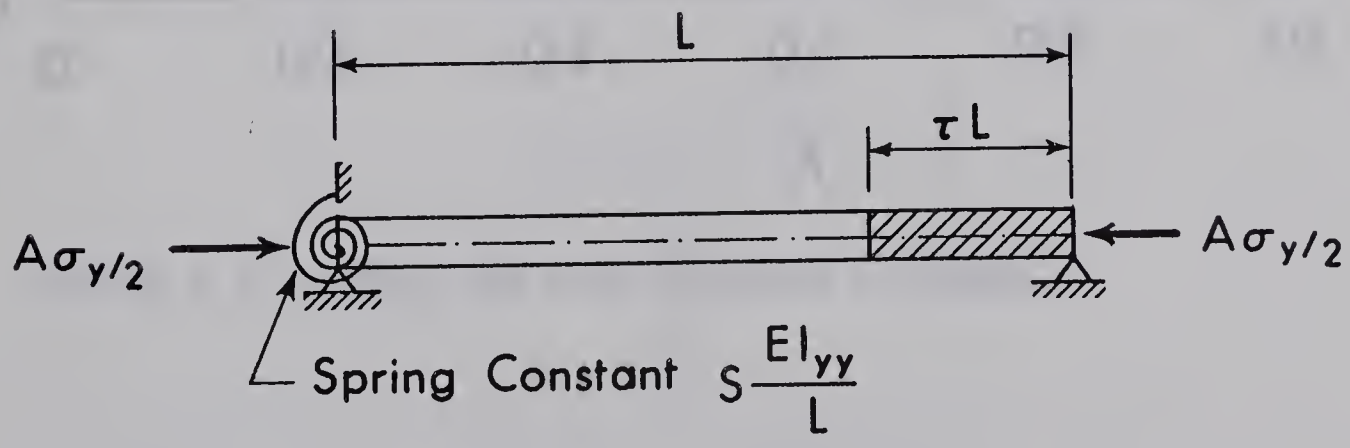

FIGURE 2.2 LATERAL BUCKLING MODEL

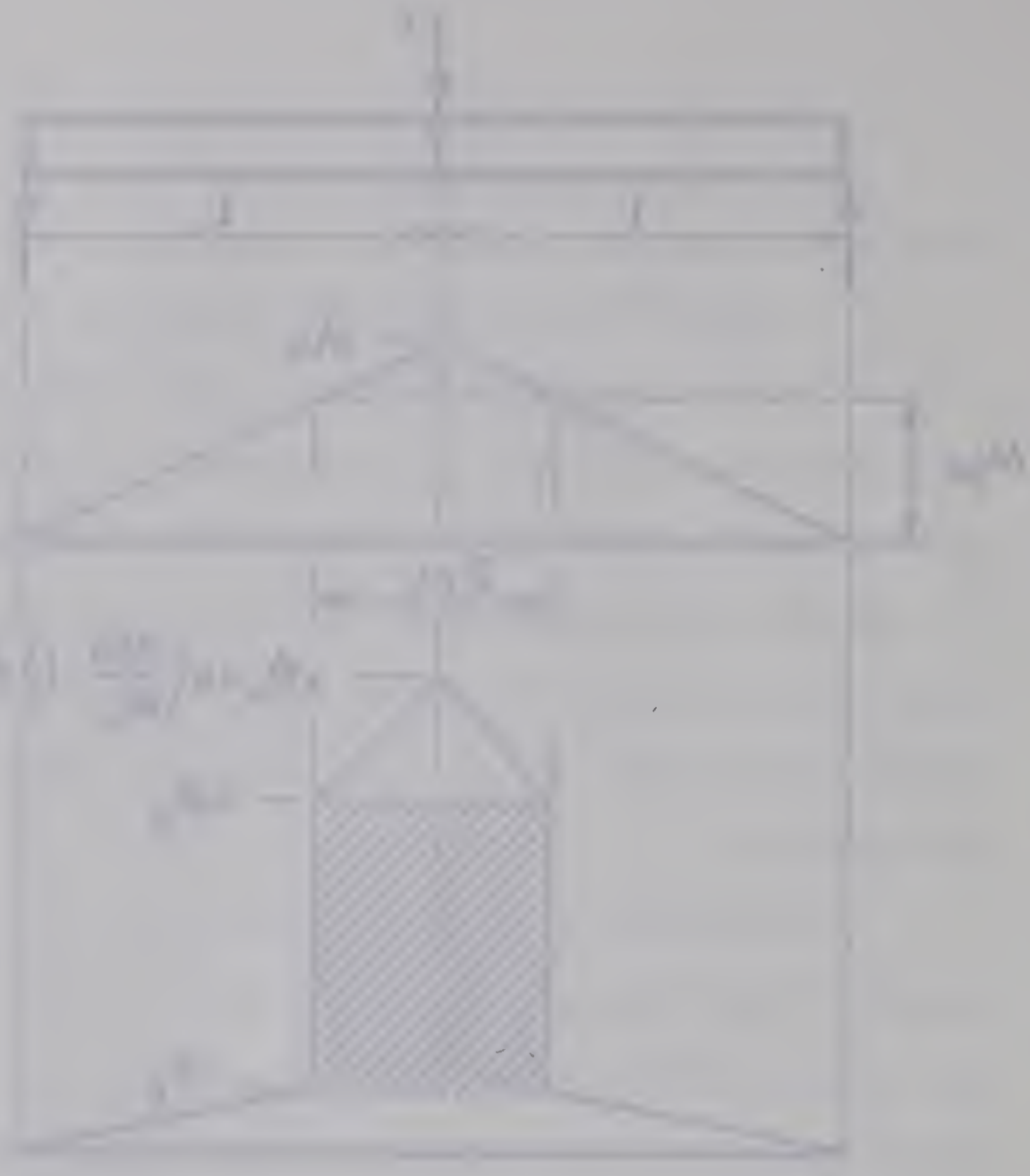

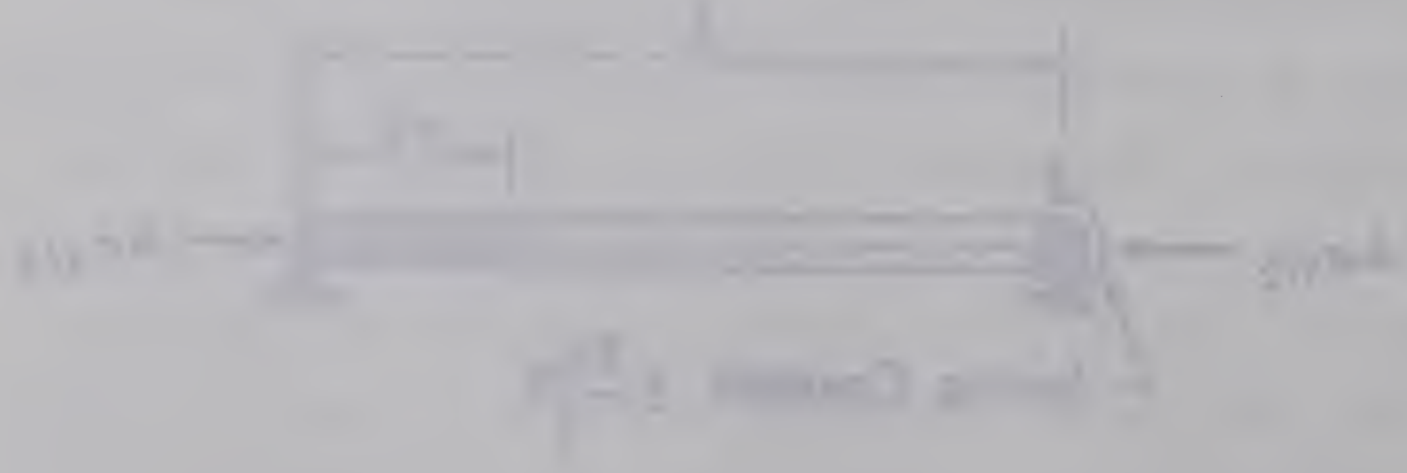

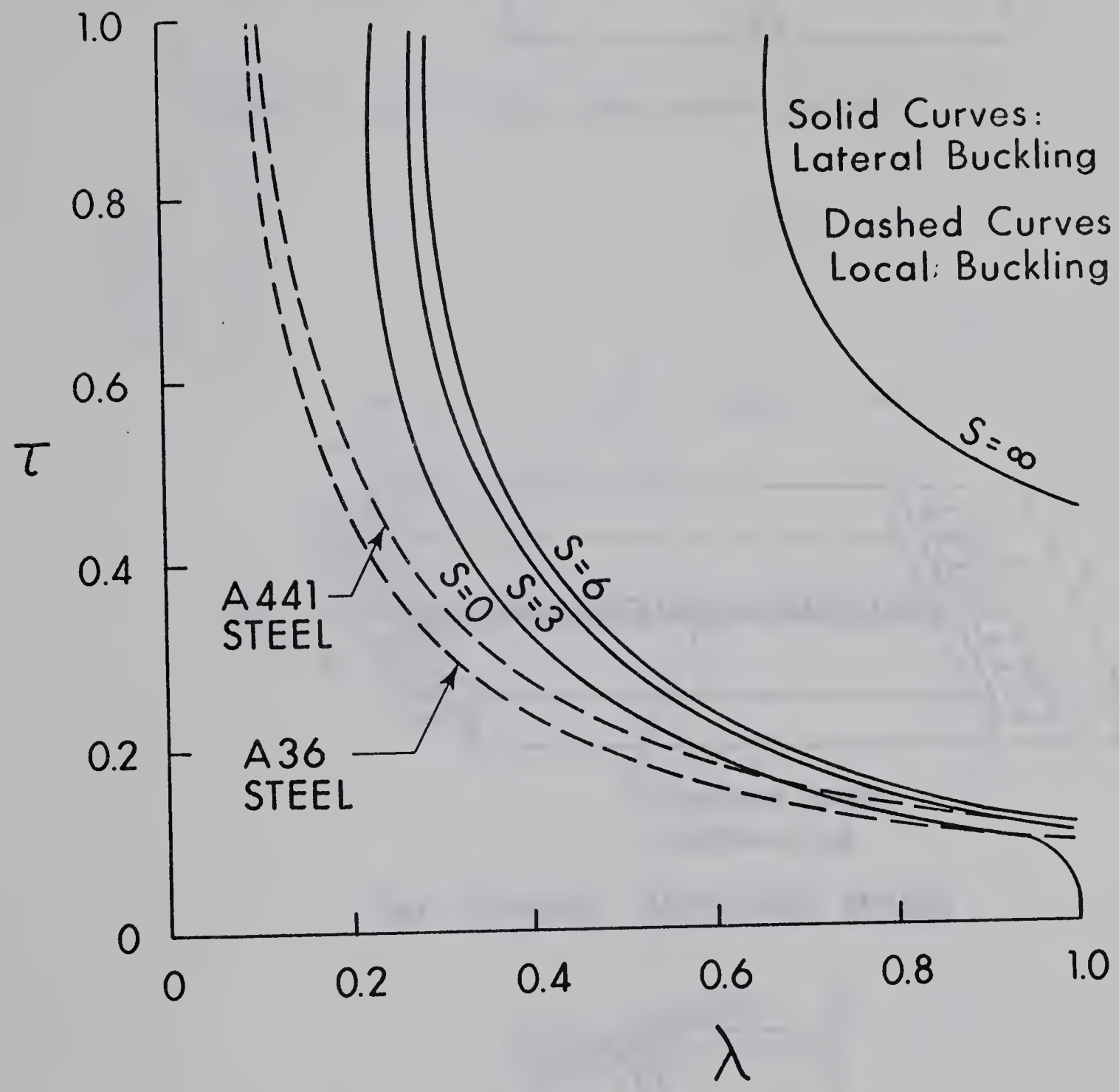

FIGURE 2.3 LATERAL AND LOCAL BUCKLING SOLUTIONS

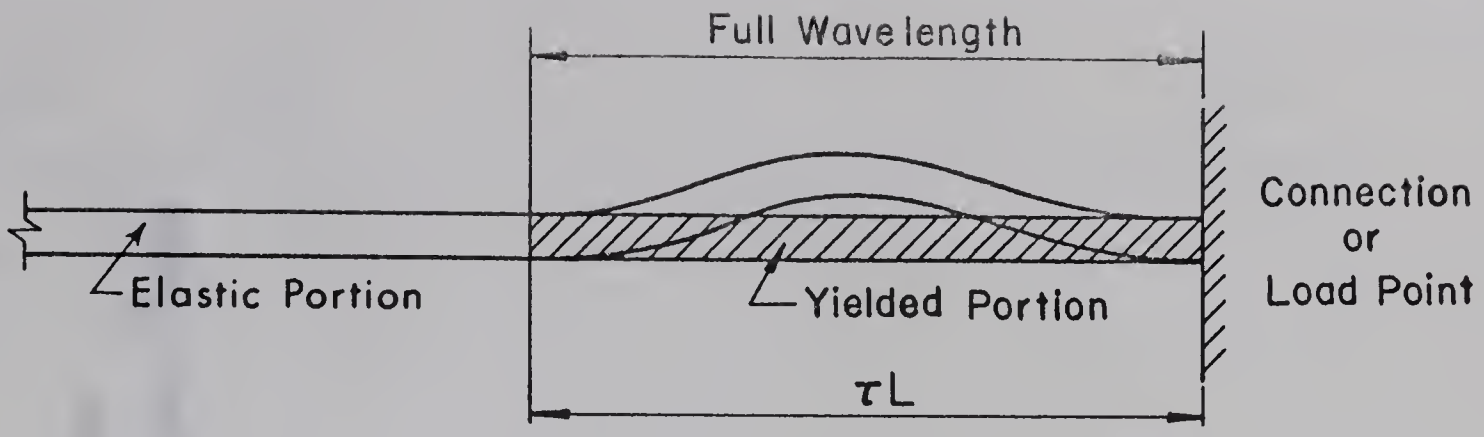

FIGURE 2.5 LOCAL BUCKLE UNDER MOMENT GRADIENT

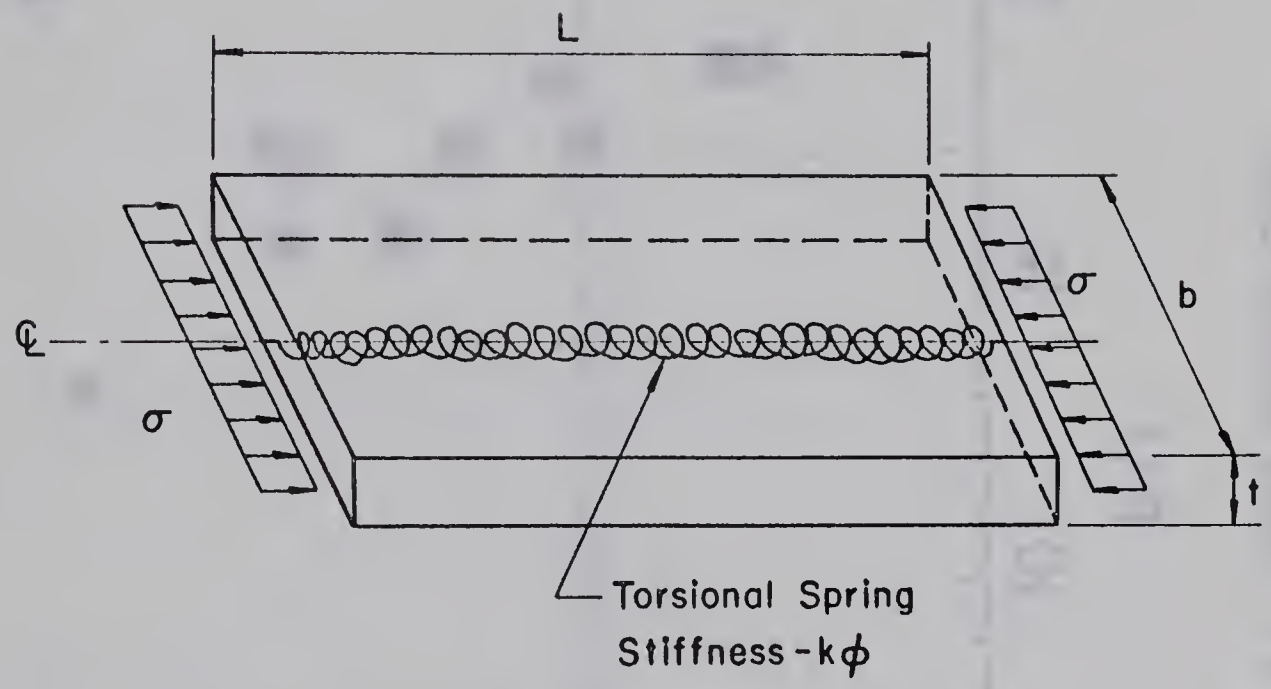

(a) FLANGE BUCKLING MODEL

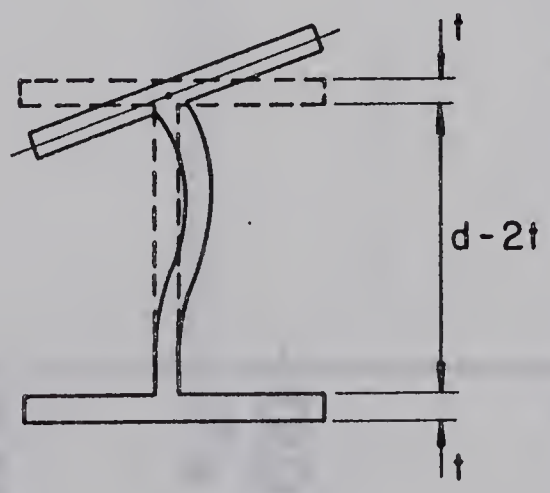

(b) WEB RESTRAINT MODEL

FIGURE 2.4 LOCAL BUCKLING MODEL

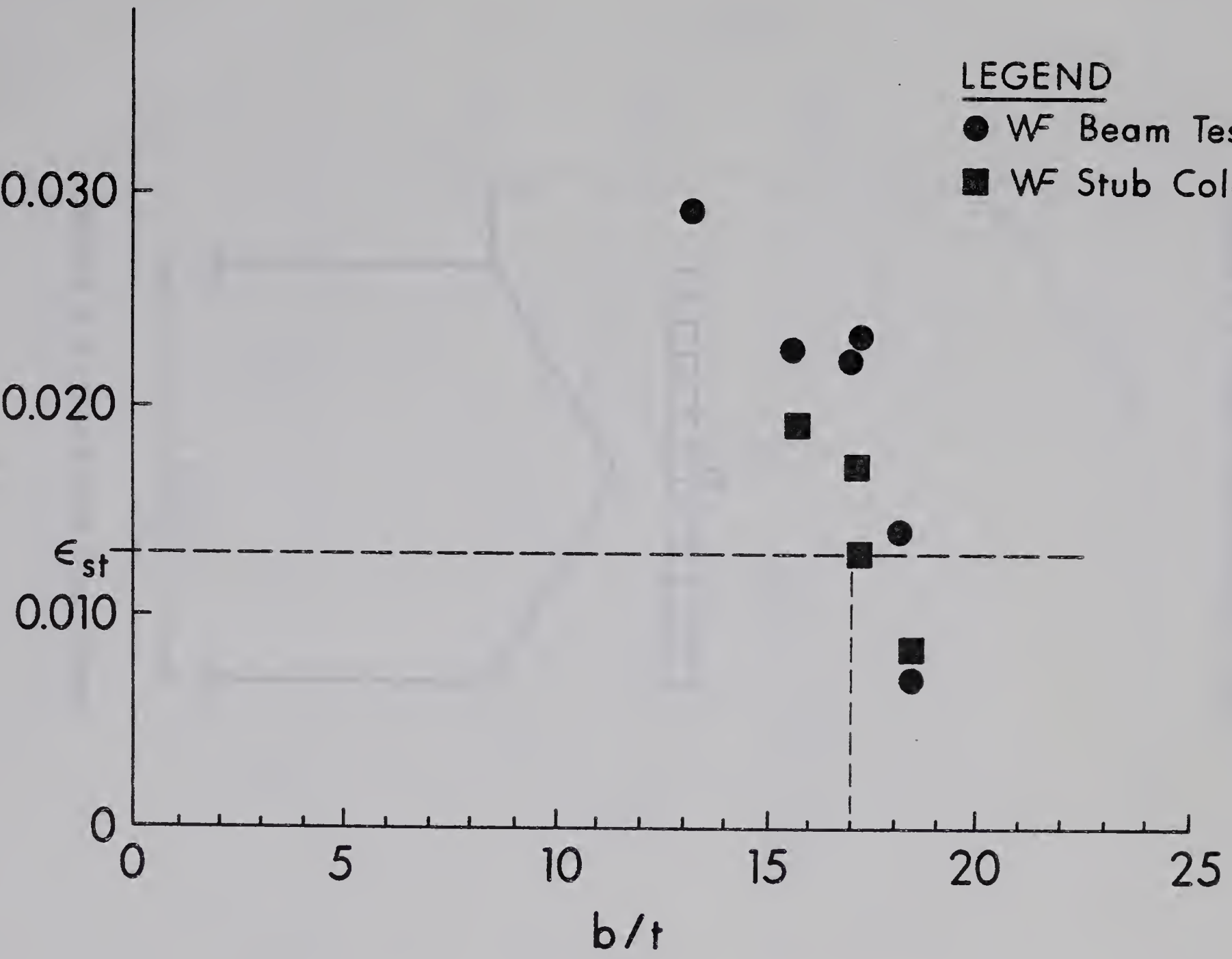

FIGURE 2.6 FLANGE BUCKLING TESTS

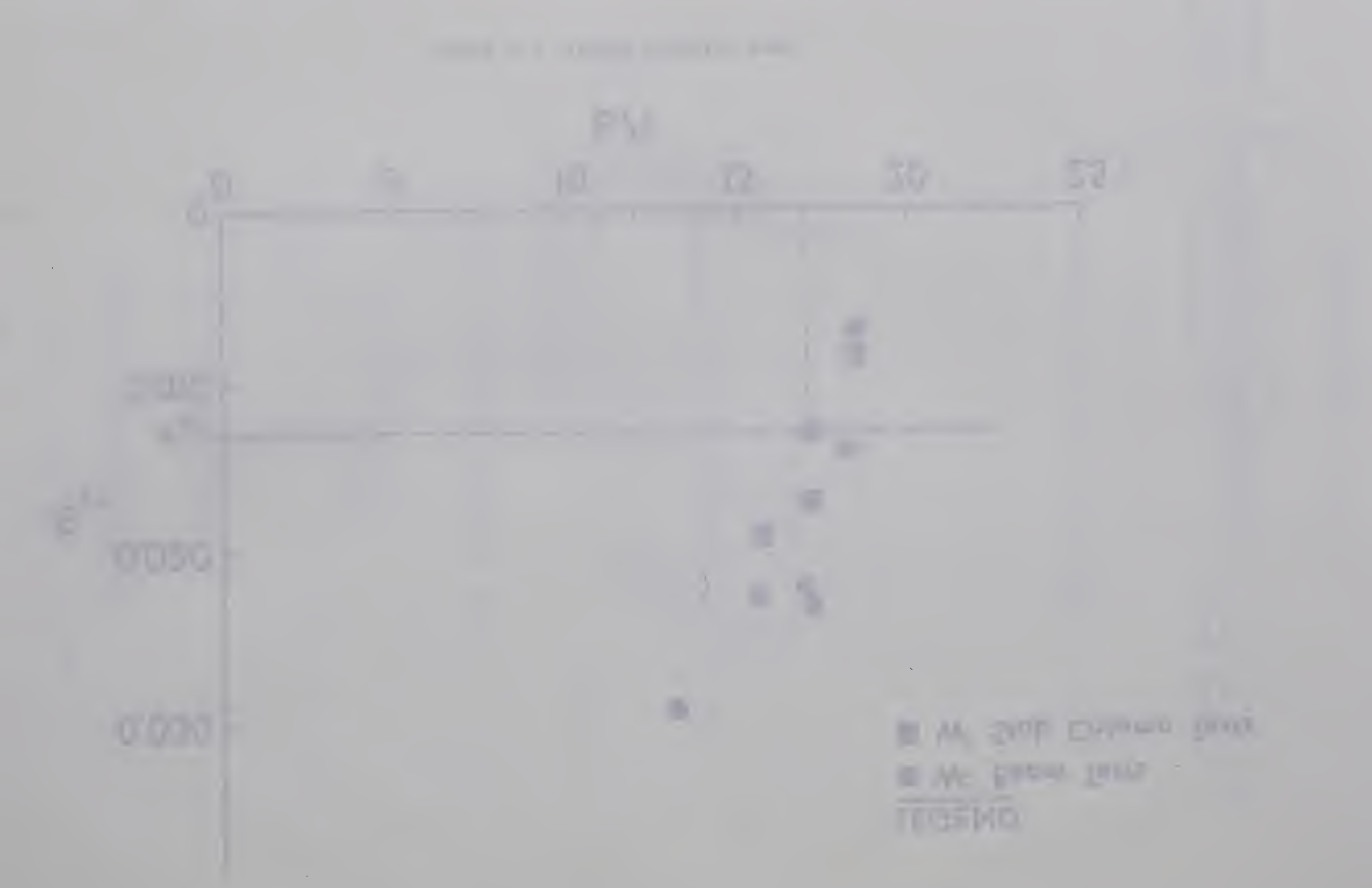

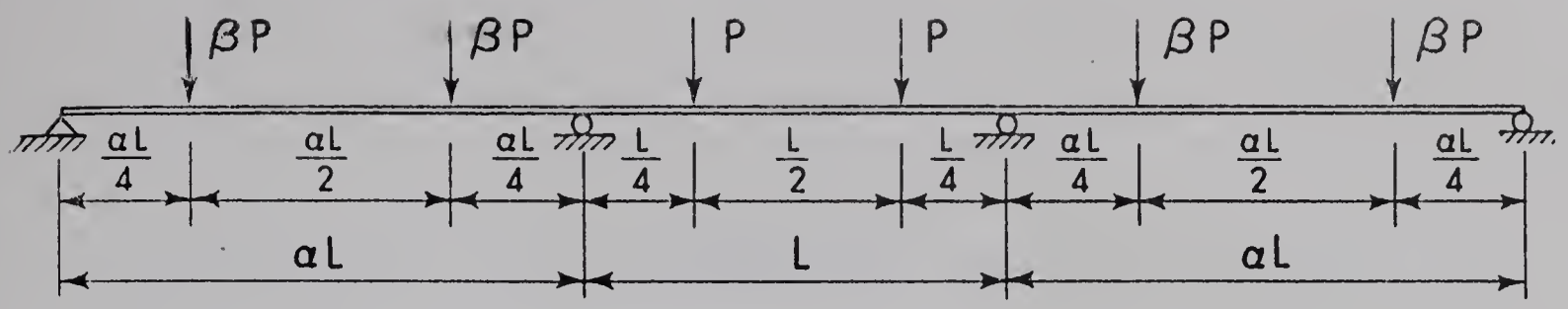

FIGURE 2.7 THREE SPAN CONTINUOUS BEAM

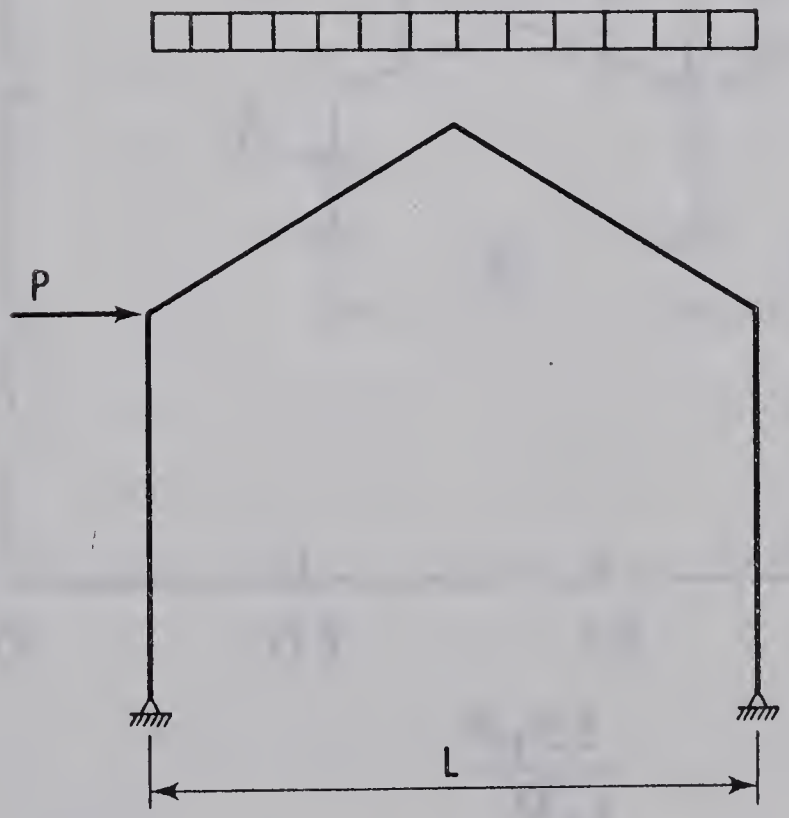

FIGURE 2.8 SINGLE SPAN RIGID FRAME

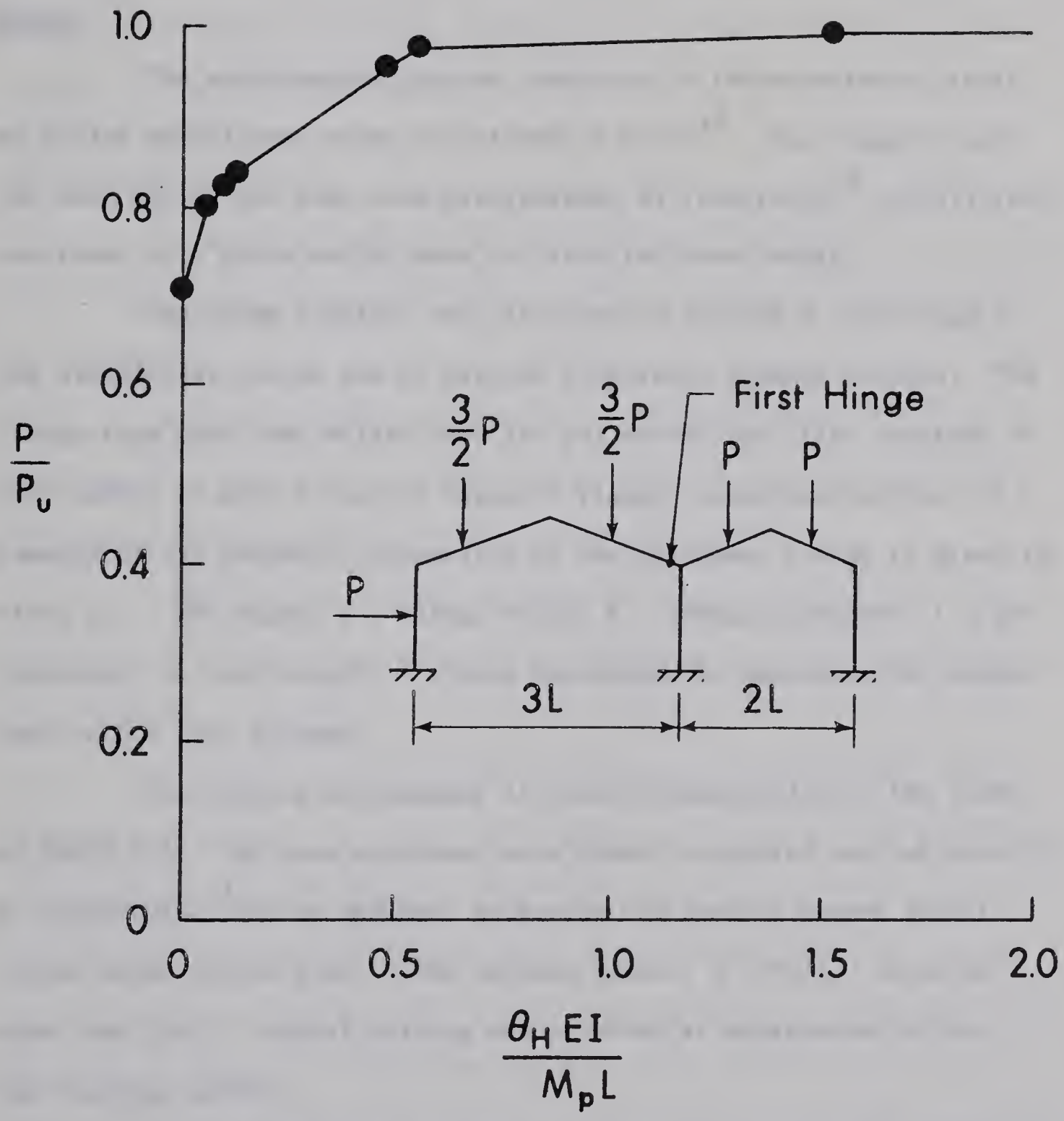

FIGURE 2.9 TWO-BAY GABLE FRAME

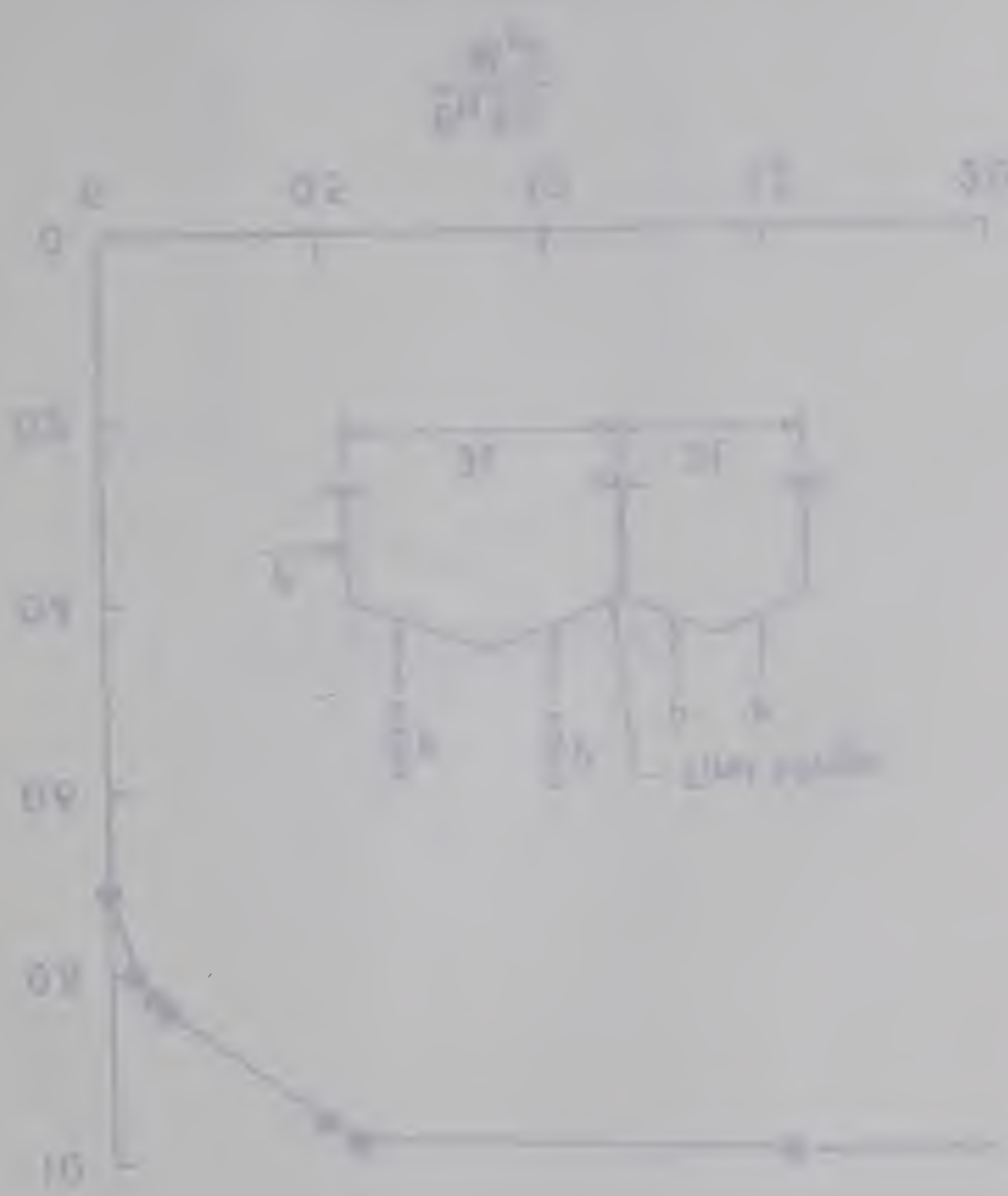

CHAPTER III

EXPERIMENTAL PROGRAM

Scope

The experimental program consisted of three series of tests on rolled wide-flange beams of CSA-G40.12 steel[18]. The lengths used for each series had been cold-straightened by rotarizing[19] and all test specimens in a given series were cut from the same length.

The three sections were selected to include a wide range of web slenderness ratios and to provide relatively slender flanges. The flange tips were then milled down for all except the first specimen in each series to give a desired range of flange slenderness ratios. A summary of the geometric properties of the specimens tested is given in TABLE 3.1. The depth, d , flange width, b , flange thickness, t , web thickness, w , and length, L , were determined by measuring the shapes used in the test program.

The testing arrangement is shown schematically in the inset to TABLE 3.1. The beam specimens were simply supported and subjected to a concentrated load at midspan, producing the bending moment distribution shown in the inset. The maximum moment, $M = PL/2$, occurred under the load. Lateral bracing was provided at midspan and at the two reaction points.

Each of the three series, A, B, and C, indicated in TABLE 3.1

was chosen to provide a particular web slenderness ratio (d/w). The flange slenderness ratio (b/t) was varied in each series by decreasing the flange width, b . The weak axis slenderness ratio (L/r_y) of the beam was maintained virtually constant for all tests by changing the length, L , as b was varied.

Material Properties

The chemical composition and mill test results for each of the three lengths are given in TABLE 3.2. These conform to the CSA-G40.12 specification[18].

Residual stress distributions, obtained by the method of sectioning[20], are given in FIGURE 3.1 for each of the three sections. These distributions are typical for rotarized beams[6].

TABLE 3.3 summarizes the material properties obtained from laboratory tension tests performed on specimens cut from each of the three lengths. The locations from which the coupons were taken are shown in the inset. In this table σ_y denotes the yield stress and σ_u the ultimate stress. ϵ_y is the calculated yield strain corresponding to a modulus of elasticity, E = 29,600 ksi, and a stress σ_y . ϵ_{st} is the measured strain at the onset of strain-hardening and E_{st} is the strain-hardening modulus. The tests were performed in a hydraulic testing machine using flat tensile specimens conforming to ASTM Specification A370-65[13]. In the plastic range the strain rate was reduced to zero for a period of two minutes, so that the σ_y values given in TABLE 3.3 represent the "static" yield stress after this time. The value of E_{st}

was obtained by graphically measuring the initial slope of the strain-hardening branch of the automatically-recorded load-strain curve. The hydraulic control valve was held at a constant setting in the strain-hardening range.

Testing Arrangement

FIGURES 3.2 and 3.3 show overall views of the test setup from the bottom-front and from the top-front, respectively. The specimens were tested as simply-supported beams, with the reaction forces taken by hanger rods. The rods were pin-connected to sets of lugs welded to the bottom flange of the test beam and to a reaction beam attached to the laboratory floor, as shown in FIGURE 3.2. Web stiffener plates were welded to the specimen at the supports and at midspan.

The concentrated load was applied by means of a hydraulic ram and transmitted to the beam through a box bolted to the midspan web stiffeners. The box was constructed to contact the specimen only at the stiffeners, and to provide ample clearance for buckling of the compression flange. The general arrangement can be seen in FIGURE 3.3. A close-up of the box attachment to the beam is shown in FIGURE 3.4. This loading arrangement was adopted to permit the application of reversed loadings in a future series of tests. Hydraulic pressure to the ram was provided by an air-driven pump, and regulated by adjustment of the air pressure and hydraulic line valves at a control panel.

The test specimens were braced laterally at the two reaction points and at midspan. Lateral support at the reaction points was pro-

vided by steel rods bolted in a horizontal position between the testing frame and the stiffener plates, as shown in FIGURE 3.3. At midspan, the lateral bracing mechanism shown in FIGURE 3.5 was used. This arrangement, based on Watt's straight-line mechanism[21] effectively restrained lateral movement of the compression flange while allowing free movement in the plane of the beam web.

FIGURE 3.6 shows the instrumentation used in the tests. The applied loads were determined primarily by monitoring the strains in the two reaction support rods (FIGURE 3.6(a)), which had been previously calibrated in a testing machine. In addition, independent checks on the indicated loads were made by taking readings from a 50-ton load cell in series with the ram (FIGURE 3.6(a)), by measuring the hydraulic pressure applied to the ram and by monitoring strains at the beam quarter-points (FIGURE 3.6(b)). Beam moments and applied forces were computed from the latter in the elastic range.

The instrumentation used in measuring specimen deformations is shown schematically in FIGURE 3.6(b). The vertical deflection at midspan was measured by means of a dial gage. Support settlements were also measured using dial gages, and the appropriate adjustment made to obtain the net vertical midspan deflection. Rotation gages were attached to the beam ends to measure the rotations at the supports. Lateral movements of the compression flange were measured at the beam quarter-points by means of dial gages placed horizontally between the beam and the testing frame. The relative vertical movements of the tension and

compression flanges were measured near the midspan of the beam by a dial gage placed between the flanges in a series of prepunched gage points.

The entire specimen was whitewashed before each test to aid in observing the progression of yielding.

Testing Procedure

Prior to each test the beam was loaded to one-half of the calculated "yield" load and then unloaded. This procedure was repeated several times to assure bearing in the connections and to check on the instrumentation. In the initial elastic range of the test, the specimen was deformed by increasing the hydraulic ram pressure to give predetermined load values. The load was maintained at each of these values until all readings had been taken.

After yielding had occurred, the incrementation procedure was to increase the midspan deflection to predetermined values; the flow of hydraulic fluid to the ram was then closed off for a five minute stabilization period before readings were taken. In addition to the instrument readings mentioned in the previous section, visual observations and measurements of the progression of yielding and local buckling were recorded for each increment.

The specimen was deformed well into the unloading range using the above procedure. The ram pressure was then reduced in several increments to trace the elastic unloading curve.

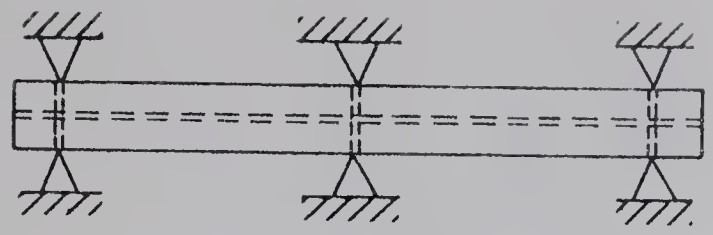

LATERAL SUPPORT

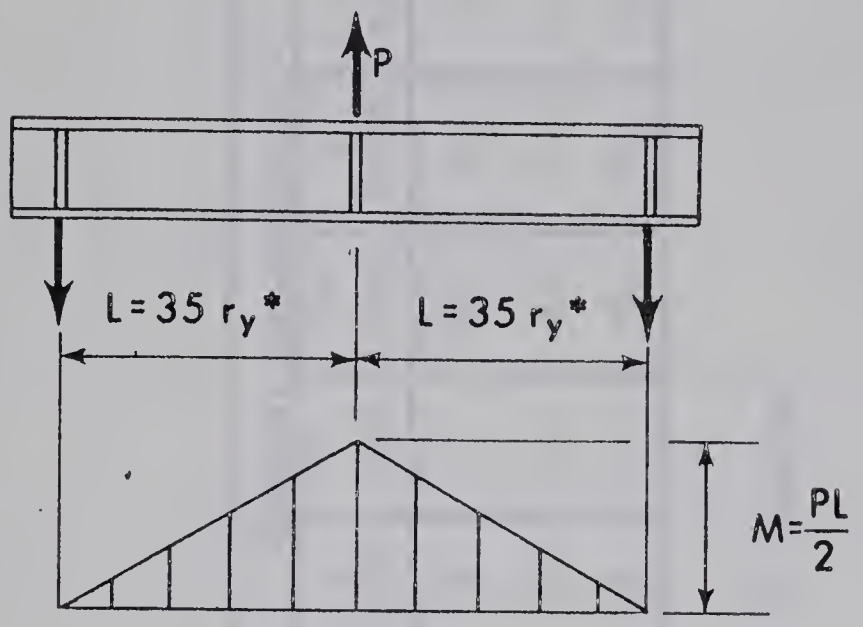

LOADING CONDITION

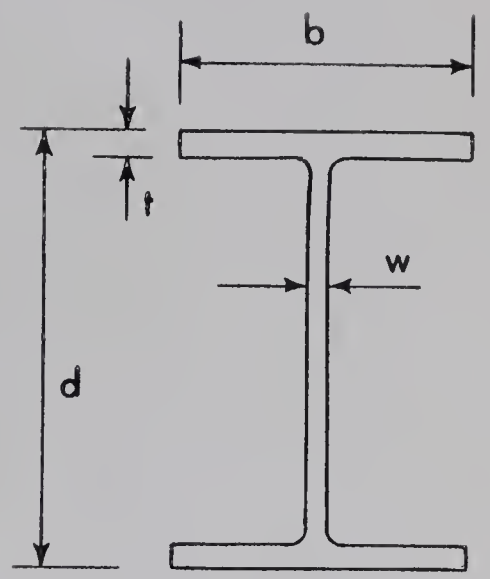

CROSS - SECTION

* NOTE:
L = 33 r_y for Specimen C-1
L = 35 r_y for all others

Test	d (in)	b (in)	t (in)	w (in)	d/w	b/t	L (in)
A-1	9.86	8.01	0.425	0.301	32.7	18.85	68.5
A-2	9.86	6.93	0.425	0.301	32.7	16.30	58.0
B-1	7.88	4.04	0.208	0.175	45.0	19.40	30.6
B-2	7.88	2.91	0.208	0.175	45.0	14.00	20.4
B-3	7.88	3.39	0.208	0.175	45.0	16.30	24.7
B-4	7.88	3.70	0.208	0.175	45.0	17.80	27.5
B-5	7.88	3.81	0.208	0.175	45.0	18.30	28.5
C-1	9.86	4.01	0.207	0.181	54.5	19.42	27.0
C-2	9.86	2.90	0.207	0.181	54.5	14.00	18.9
C-3	9.86	3.38	0.207	0.181	54.5	16.30	23.0
C-4	9.86	3.68	0.207	0.181	54.5	17.80	25.5
C-5	9.86	3.54	0.207	0.181	54.5	17.10	24.4

TABLE 3.1 TEST PROGRAM

Length	Physical Properties			Chemical Composition %				
	Yield Stress (ksi)	Ultimate Stress (ksi)	Elongation (%)	C X100	Si X100	Mn X100	P X1000	S X1000
A	47.9	70.0	21	18	6	110	10	20
B	60.7	73.4	22	18	2	81	22	25
C	58.7	75.3	22	18	3	94	26	24

TABLE 3.2 CHEMICAL COMPOSITION AND MILL TEST RESULTS

Series	Coupon	σ_y (ksi)	$\epsilon_y = \sigma_y / E^*$	ϵ_{st}	E_{st} (ksi)	σ_u (ksi)	% Elongation
A	F1	40.2	0.00136	0.0134	836	69.0	27
	F2	40.8	0.00138	0.0150	767	69.2	29
	F3	42.1	0.00142	0.0082	888	69.5	25
	F4	42.2	0.00143	0.0119	729	69.5	30
	W5	45.1	0.00152	0.0096	488	--	25
	W6	44.6	0.00151	0.0134	575	69.8	26
B	F1	54.3	0.00183	0.0276	453	70.9	20
	F2	52.2	0.00176	0.0272	442	72.6	23
	F3	56.0	0.00189	0.0240	458	69.6	24
	F4	53.9	0.00182	0.0288	484	71.4	22
	W5	59.6	0.00202	0.0247	489	77.5	16
	W6	55.4	0.00187	0.0240	443	77.0	20
C	F1	55.1	0.00186	0.0215	476	74.3	24
	F2	52.5	0.00177	0.0216	524	72.7	25
	F3	53.4	0.00180	0.0218	591	74.4	26
	F4	55.5	0.00188	0.0234	466	77.2	23
	W5	50.3	0.00170	0.0238	481	70.0	20
	W6	51.8	0.00175	--	-	70.4	19

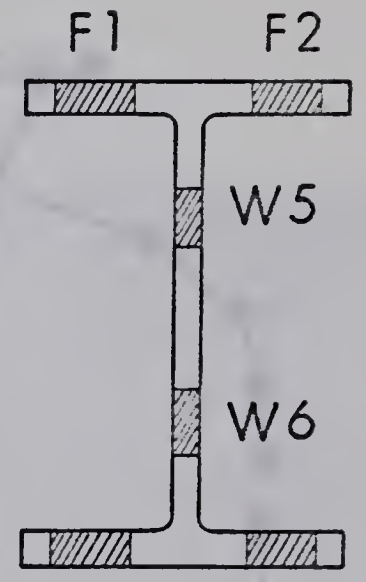

*Note - E taken as 29.6×10^3 ksi

TABLE 3.3 MATERIAL PROPERTIES


F1
F2
W5
W6
F3
F4
COUPON
LOCATIONS

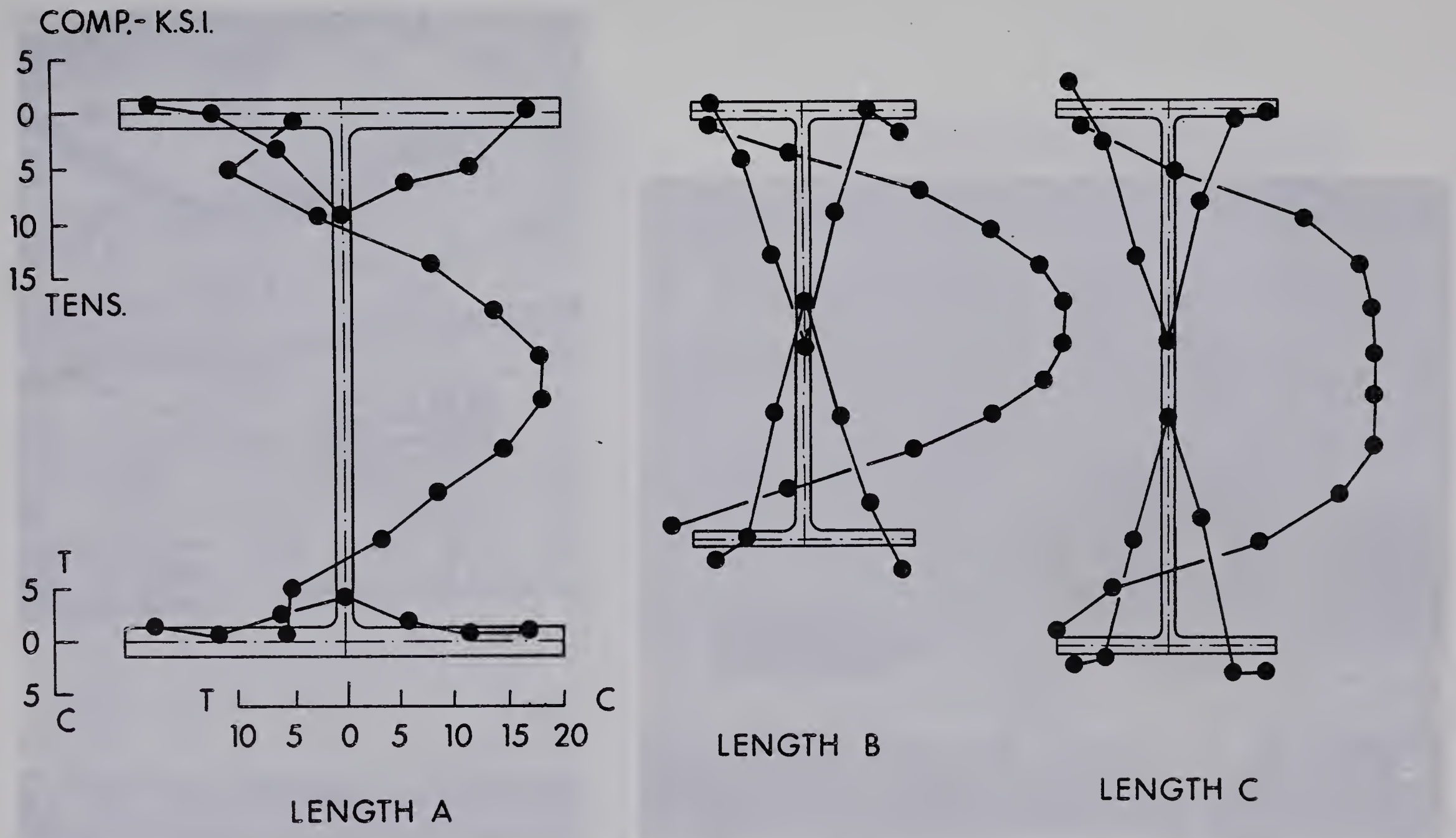

FIGURE 3.1 RESIDUAL STRESSES


АБВГ
10
0
2

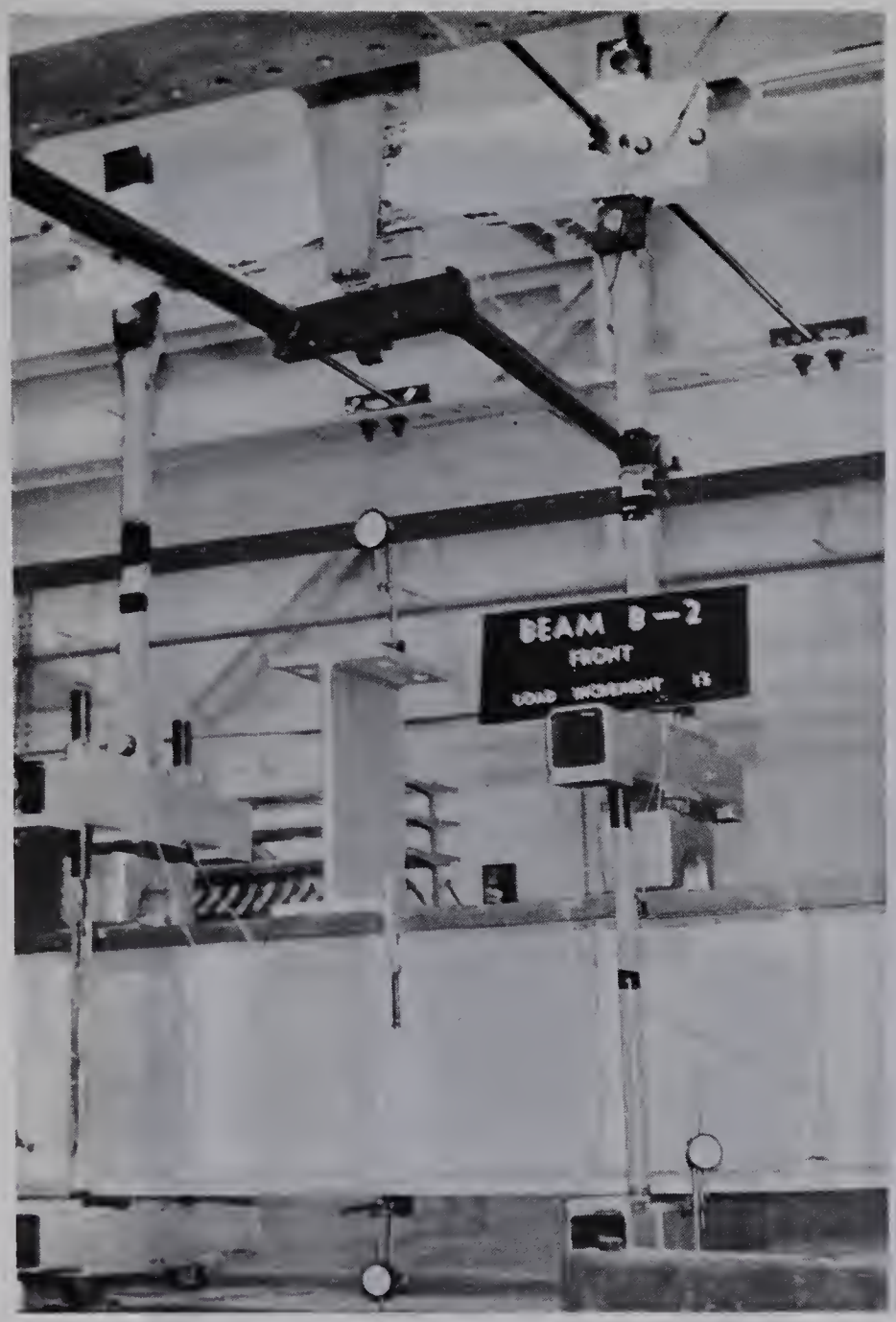

FIGURE 3.2 TEST SETUP - BOTTOM FRONT VIEW

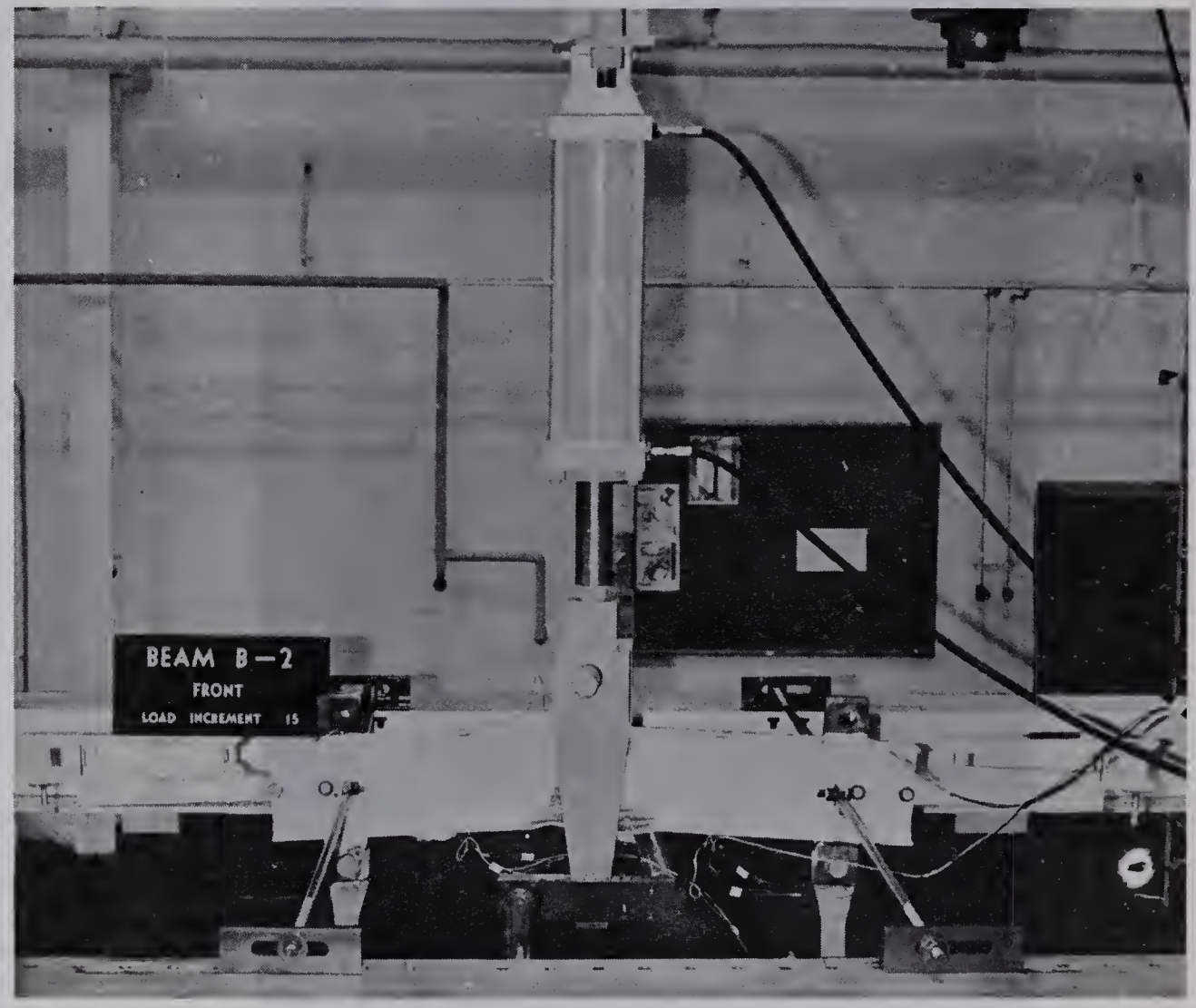

FIGURE 3.3 TEST SETUP - TOP FRONT VIEW

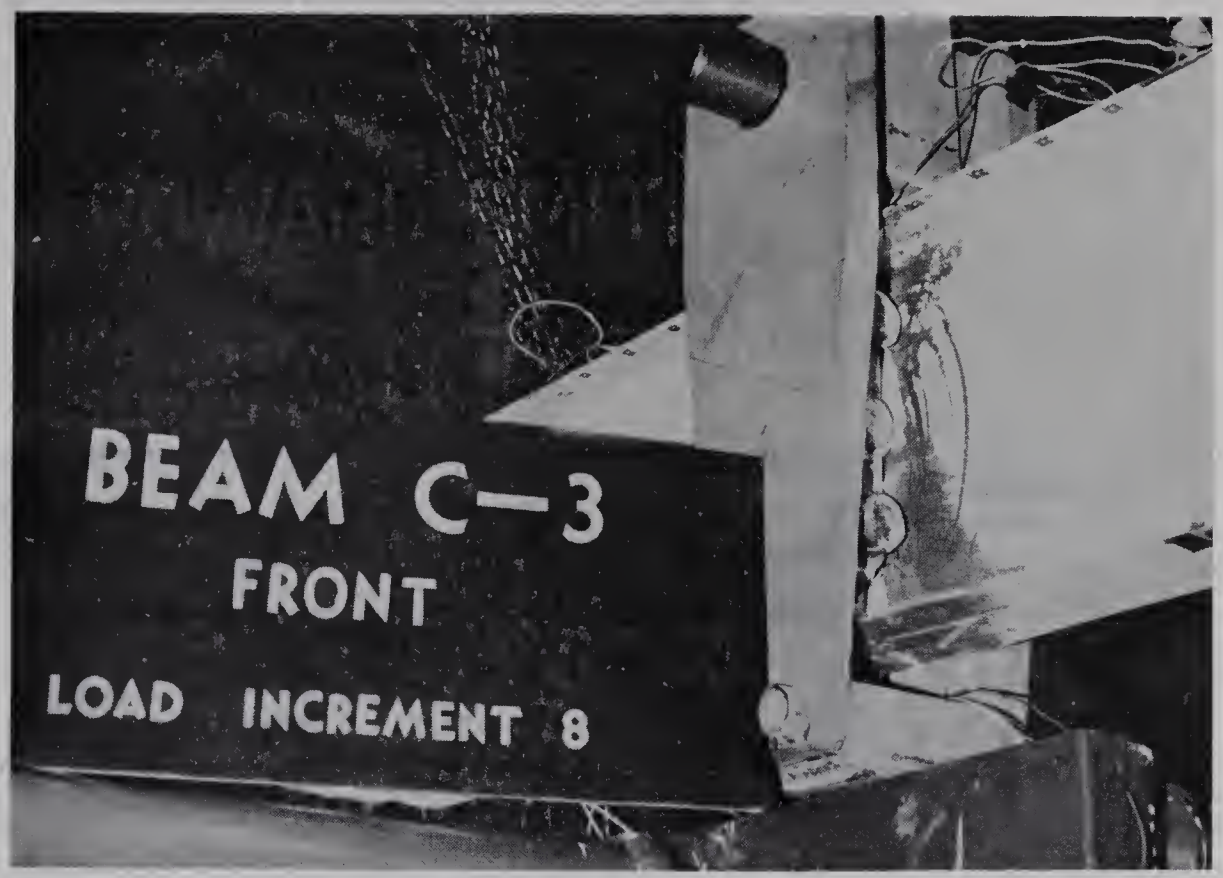

FIGURE 3.4 LOADING BOX ATTACHMENT TO BEAM

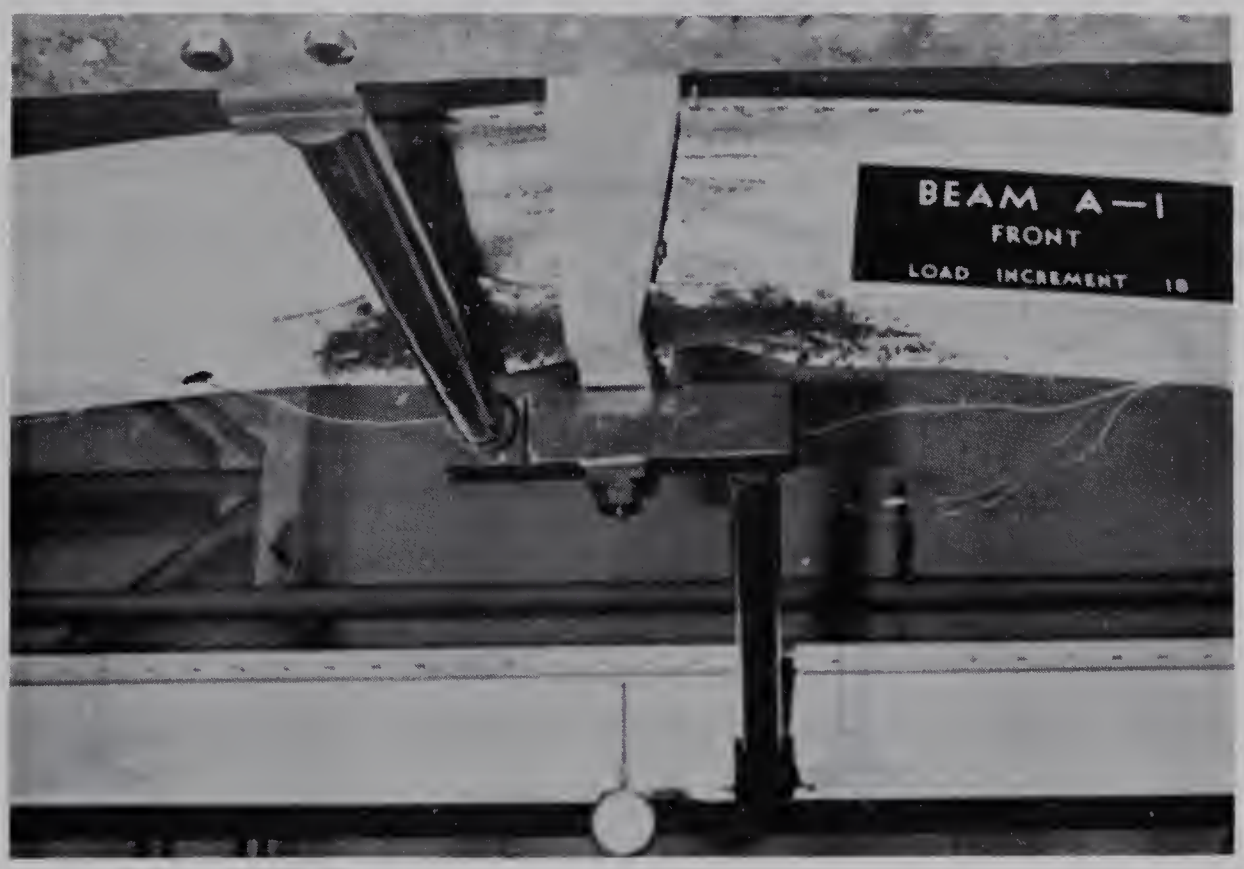

FIGURE 3.5 MIDSPAN LATERAL BRACE

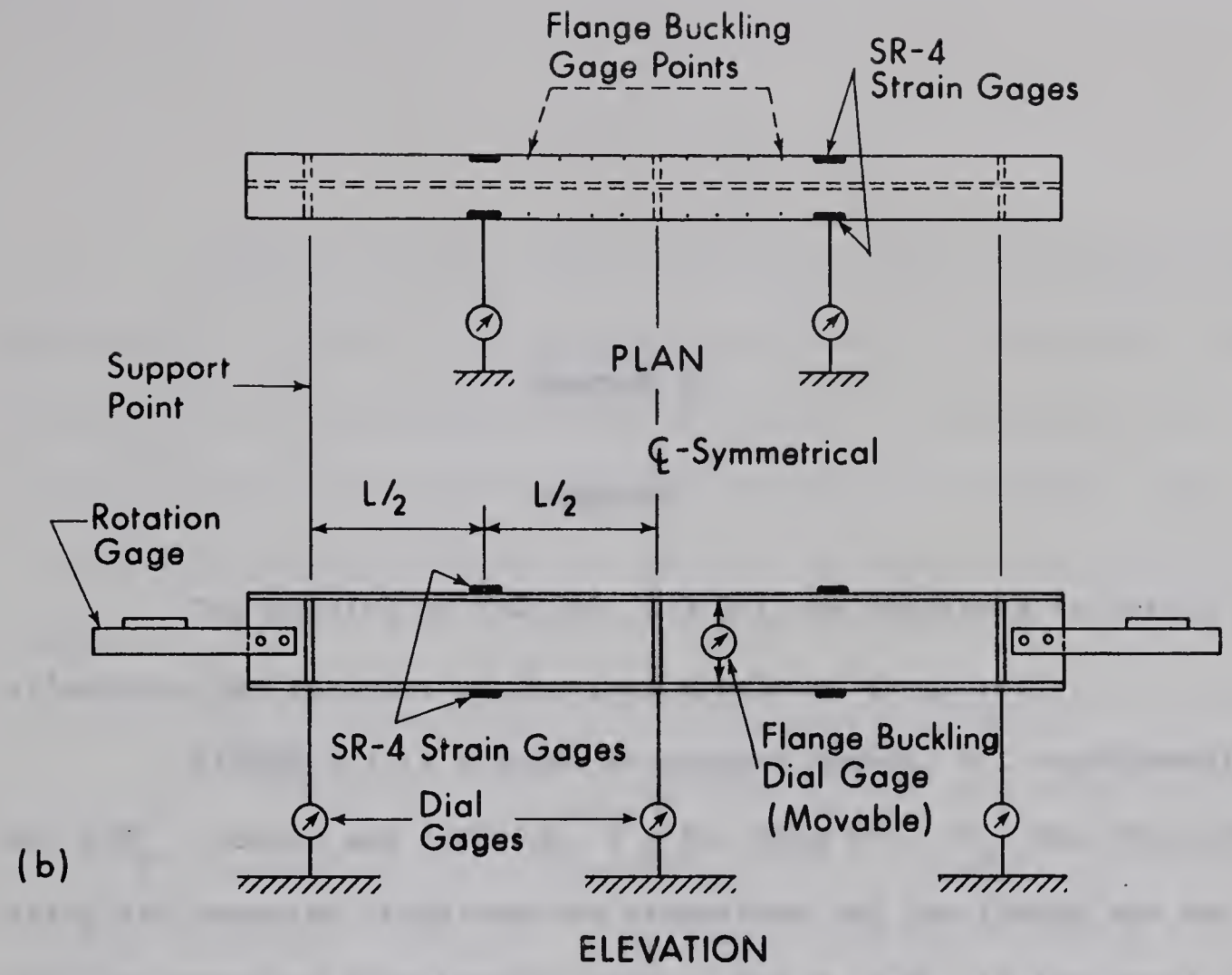

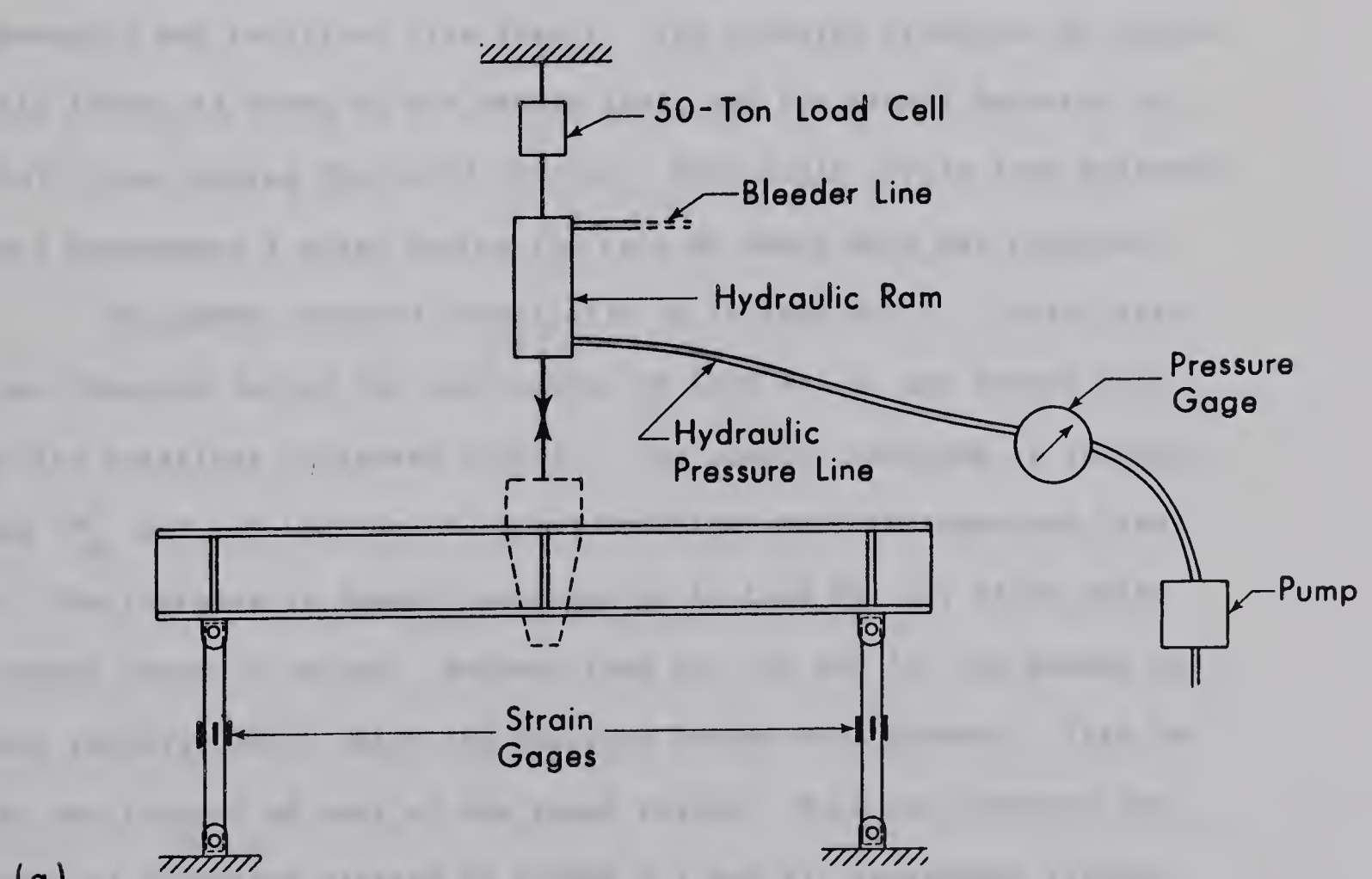

FIGURE 3.6 INSTRUMENTATION

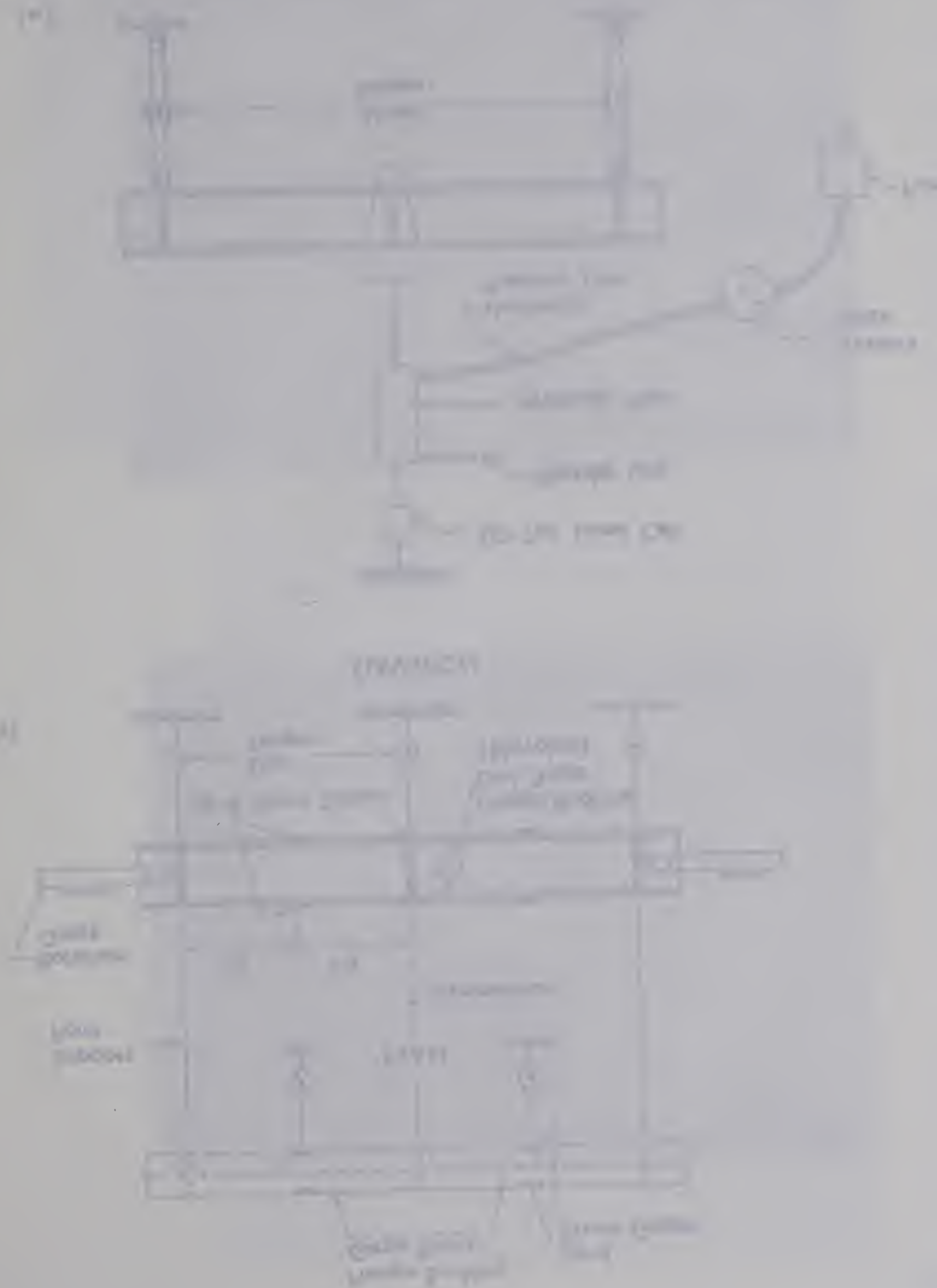

CHAPTER IV

RESULTS

The results of Test No. B-3 will be described in detail to illustrate the behavior of the test specimens in general.

FIGURE 4.1 is a graph of midspan moment, M , non-dimensionalized as M/M_p , versus end rotation, Θ , for beam B-3. M_p was calculated using the measured cross-section dimensions and the flange and web yield stresses obtained from tension tests. $\Theta = \Theta_L + \Theta_R$ is the total of the two measured end rotations (see inset). The behavior predicted by simple plastic theory is shown as the dashed line, and the actual behavior as the full line joining the solid circles. Each solid circle (and adjacent number) represents a stage during the test at which data was recorded.

The member behaved elastically up to Load No. 4. First yielding was observed during the application of Load No. 5, and beyond this stage the rotations increased rapidly. The moment continued to increase beyond M_p and, at Load No. 8, local buckling was first observed visually. The increase in moment continued up to Load No. 10, after which the member began to unload. Between Load Nos. 10 and 12, the moment decreased rapidly, after which the decrease became more gradual. This behavior was typical of most of the beams tested. Both the observed and theoretical rotations plotted in FIGURE 4.1 and all subsequent figures exclude the effects of shear deformations[10].

FIGURE 4.2 plots M/M_p versus the vertical deflection at midspan for beam B-3. The full line represents the actual beam behavior (including shear deformations) and the dashed line represents the elastic-plastic prediction with shear deformations included. The experimental curve is similar in shape to the $M/M_p - \theta$ curve described above.

The local buckling deformations of the compression flange are shown in FIGURE 4.3. This figure plots M/M_p versus the out-of-plane displacement of the compression flange tips at two gage points on opposite sides of the web. The change in distance between the tension and compression flanges was measured with a dial gage, as shown in the inset; this change was taken to represent the out-of-plane displacement of the compression flange tips. The two gage points for which the deflections are plotted are those which had the largest observed deformations. The first pronounced evidence of flange displacement at these points occurred at Load No. 9, while local buckling was first observed visually at Load No. 8. This was due to the fact that the initial buckling configuration did not extend to the points at which measurements were taken. Buckling deformations increased rapidly beyond Load No. 9. For this beam, as for all others in the test series, the out-of-plane movement was greatest in the direction toward the tension flange. FIGURE 4.4 shows the local buckling deformations at various loading increments. The numbers shown in the photographs correspond to the load numbers shown in FIGURE 4.1

FIGURE 4.5 shows a graph of M/M_p versus the lateral displacements of the compression flange quarter-points, as shown in the inset. The first pronounced movement occurred at Load No. 8, corresponding to the initiation of local buckling. Beyond this point lateral deformations increased rapidly, and the combined lateral and local buckling deformations were accompanied by an eventual drop in moment capacity. For this beam, the lateral displacement of one of the quarter-points (left) was considerably greater than the other (right) because of the fact that local buckling occurred primarily on the left side of midspan. A similar situation occurred in a number of the tests, although some did deform almost symmetrically about midspan. In all tests, the compression flange deflected laterally into an "S" shape, as may be seen for the Series B specimens in FIGURE 4.6.

The experimental moment-rotation relationships for all 12 beams tested are summarized in FIGURES 4.7, 4.8 and 4.9 for Series A, B, and C, respectively. M/M_p is plotted against the dimensionless rotation parameter, θ/θ_p, where $\theta_p = M_p L/EI$. The point at which local buckling was first observed visually is indicated on each curve.

In FIGURE 4.7 it is seen that the difference between the most slender-flanged beam, A1 ($b/t = 18.8$), and the just-compact[1] beam, A2 ($b/t = 16.3$), is relatively minor. Both specimens delivered large rotations at moments exceeding M_p. Therefore no specimens having intermediate b/t values were tested in Series A.

In Series B and C the range of b/t ratios tested was from 14.0 to 19.4. The value of 14.0 is slightly lower than the limit for

compact sections given by Reference 1. This limit is based on the measured value of σ_y for the flanges. FIGURES 4.8 and 4.9 show the large variations in rotation capacity which occurred within this range of b/t values for both Series B and Series C. In each of these series, three intermediate tests were performed on specimens having b/t values between the two extremes in order to define the relationship between b/t and rotation capacity in this range.

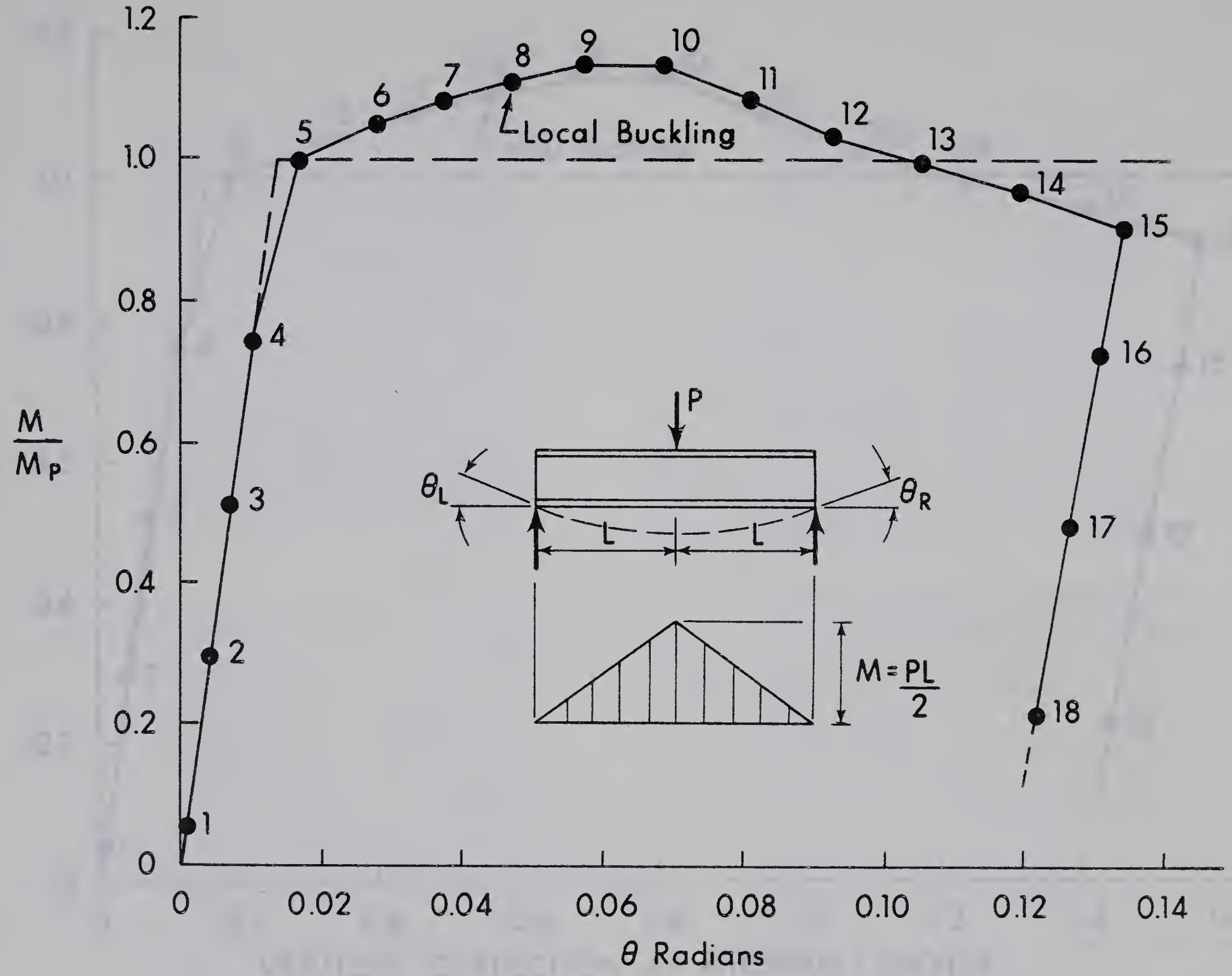

FIGURE 4.1 MOMENT-ROTATION RELATIONSHIP FOR BEAM B-3

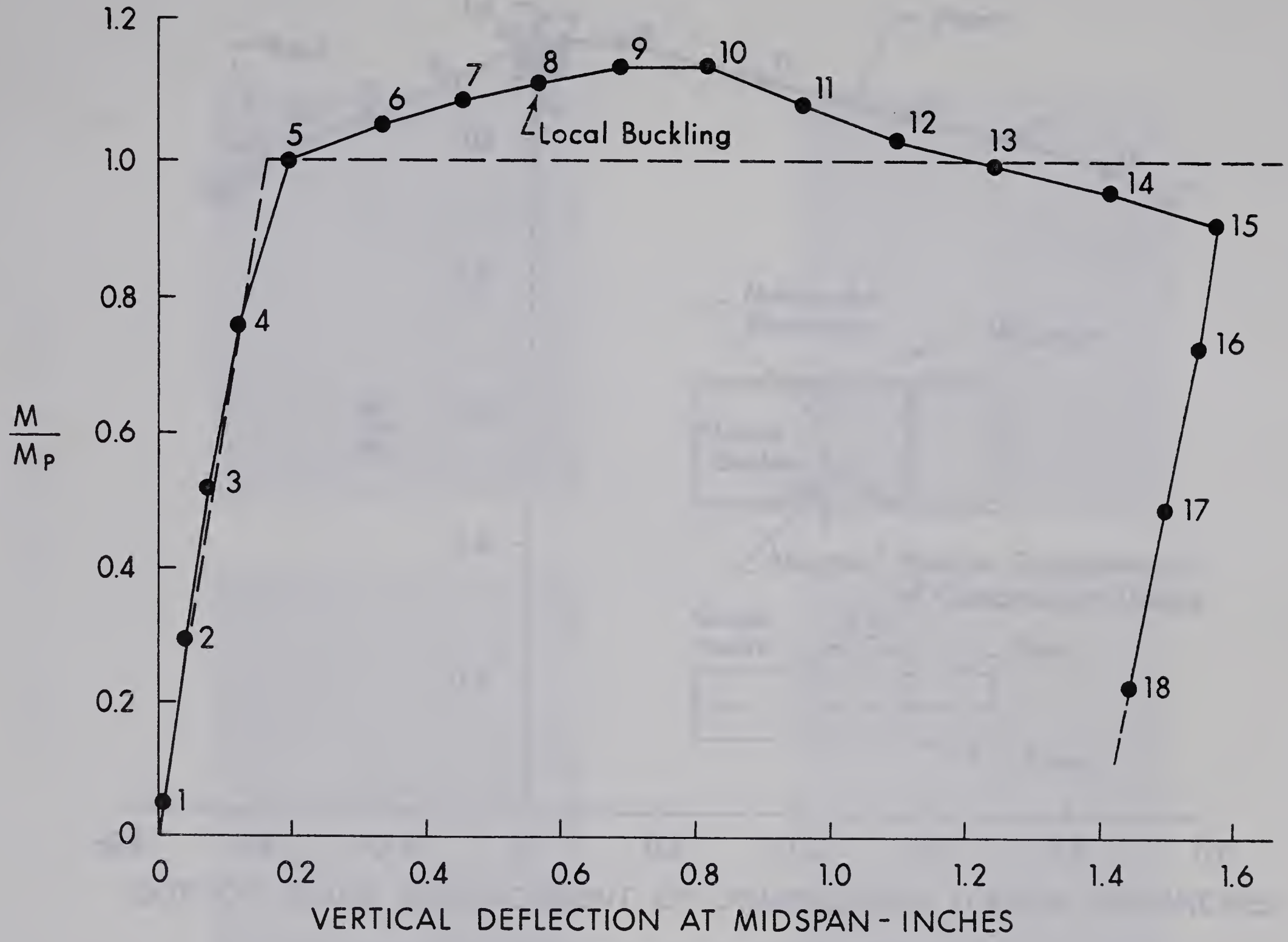

FIGURE 4.2 MOMENT-DEFLECTION RELATIONSHIP FOR BEAM B-3

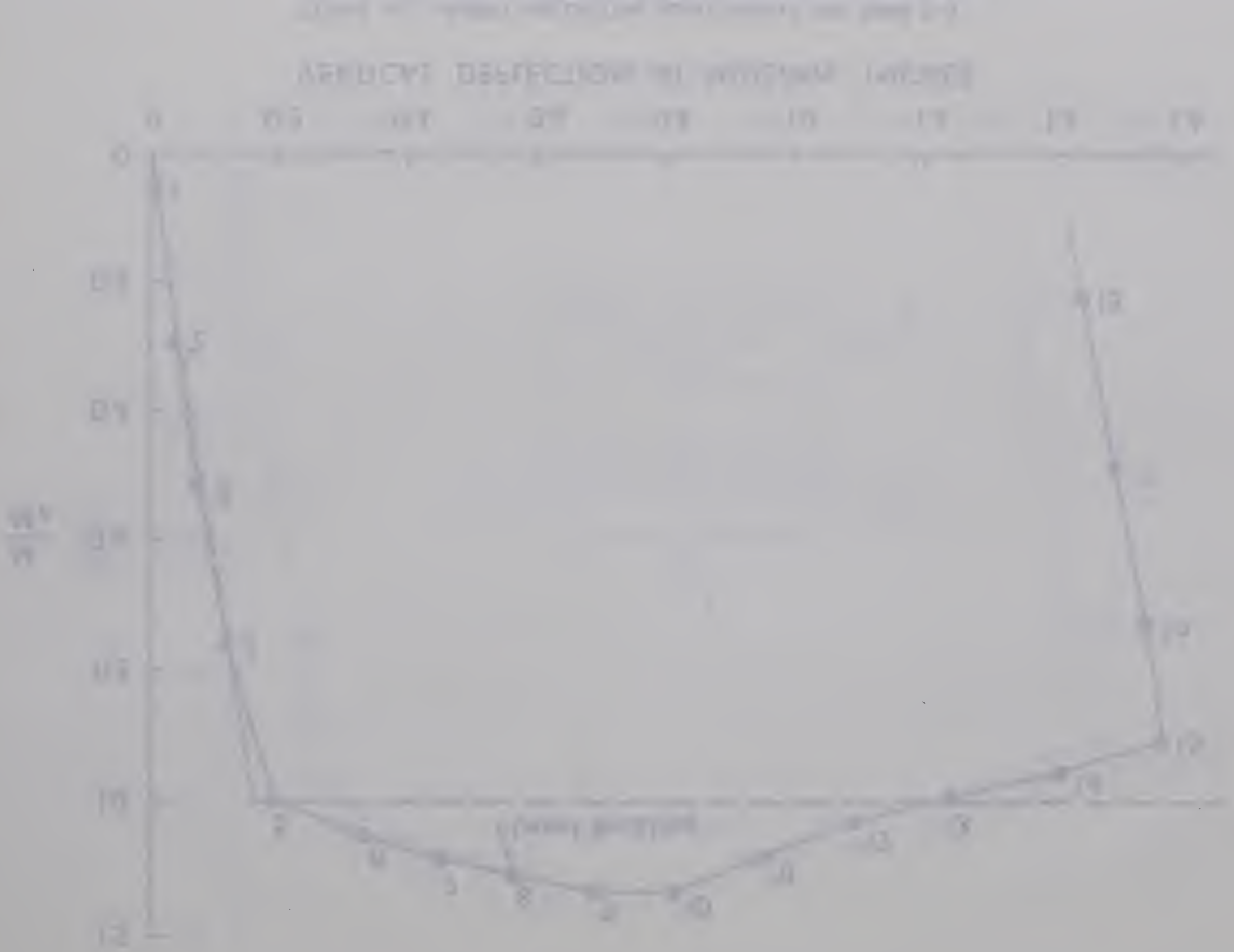

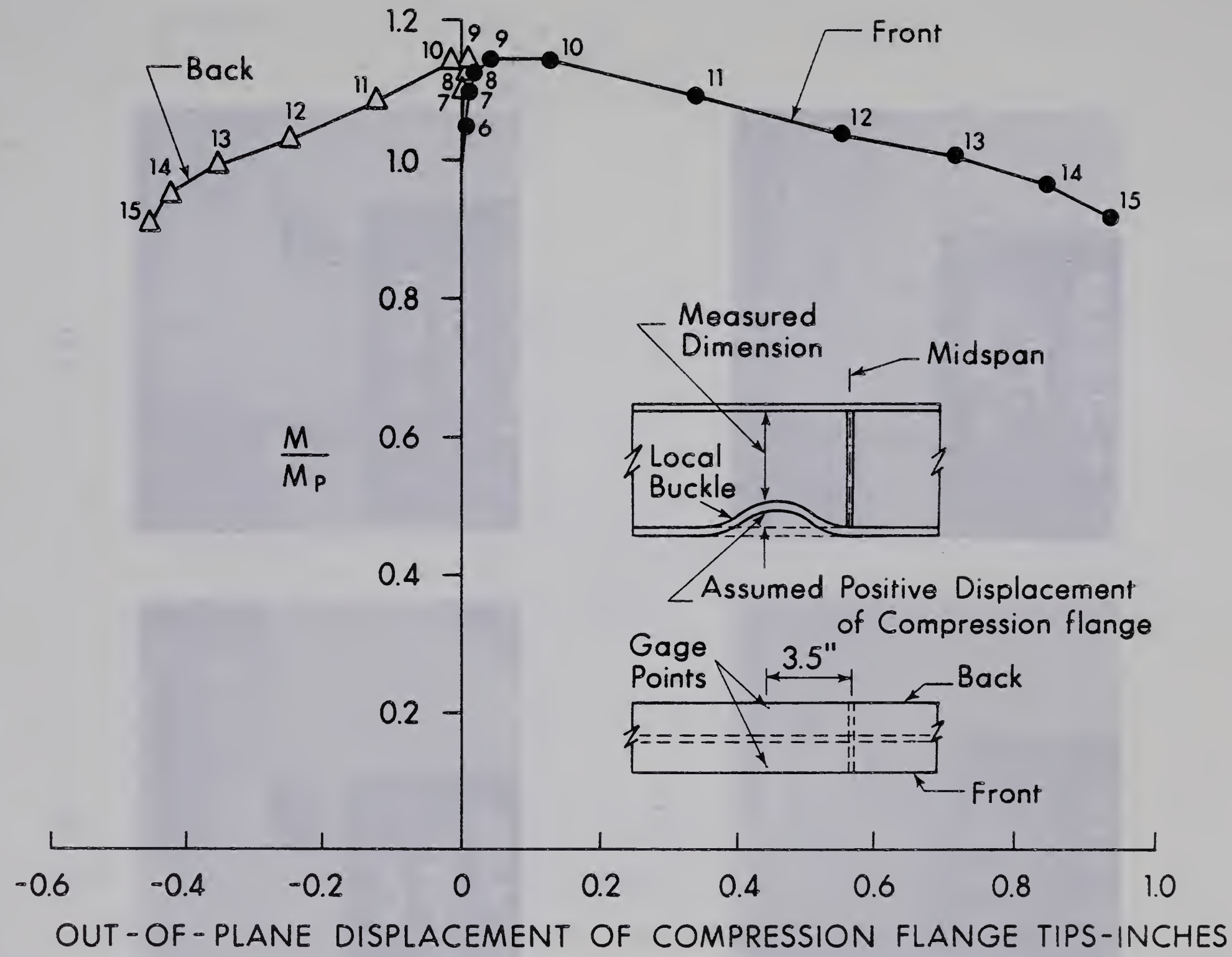

FIGURE 4.3 LOCAL BUCKLING DEFLECTIONS - BEAM B-3

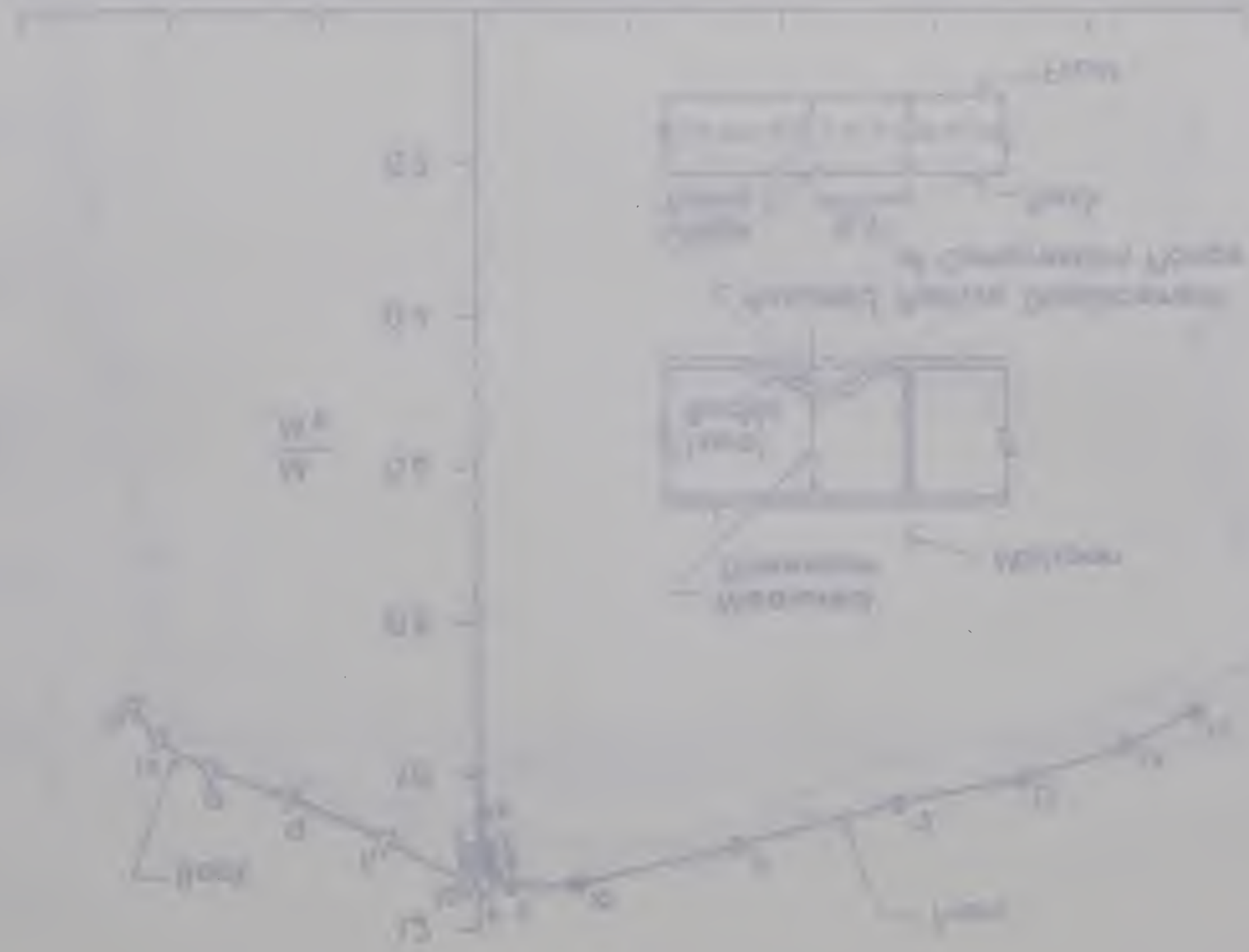

(a)

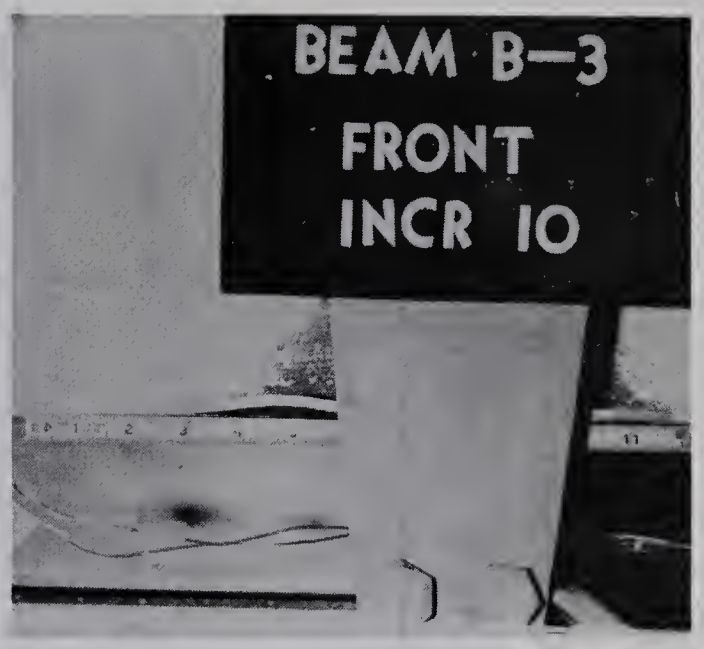

(b)

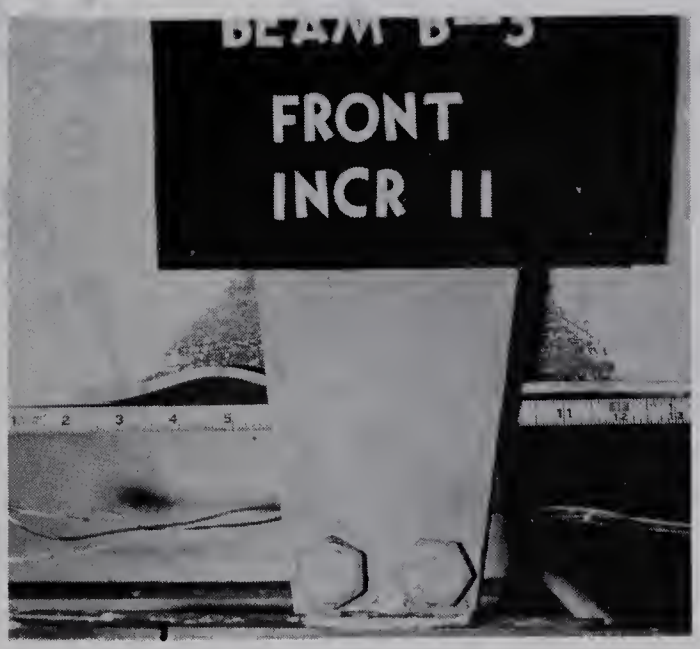

(c)

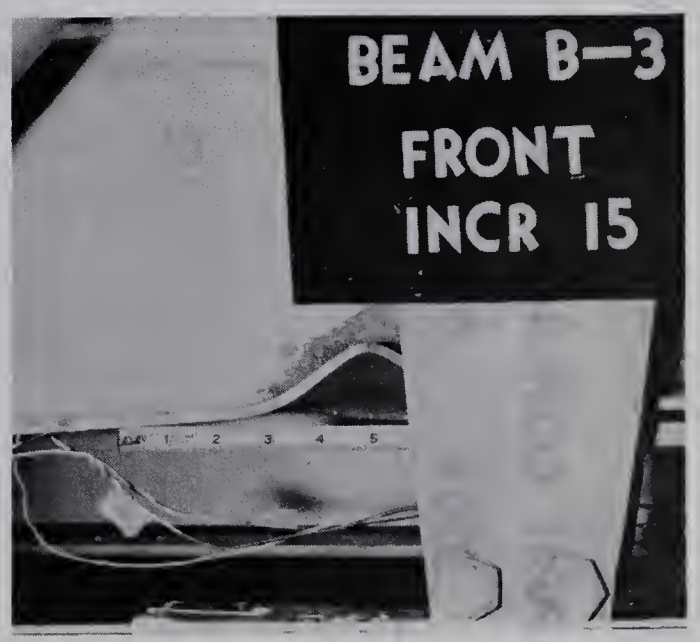

(d)

FIGURE 4.4 LOCAL BUCKLING - BEAM B-3

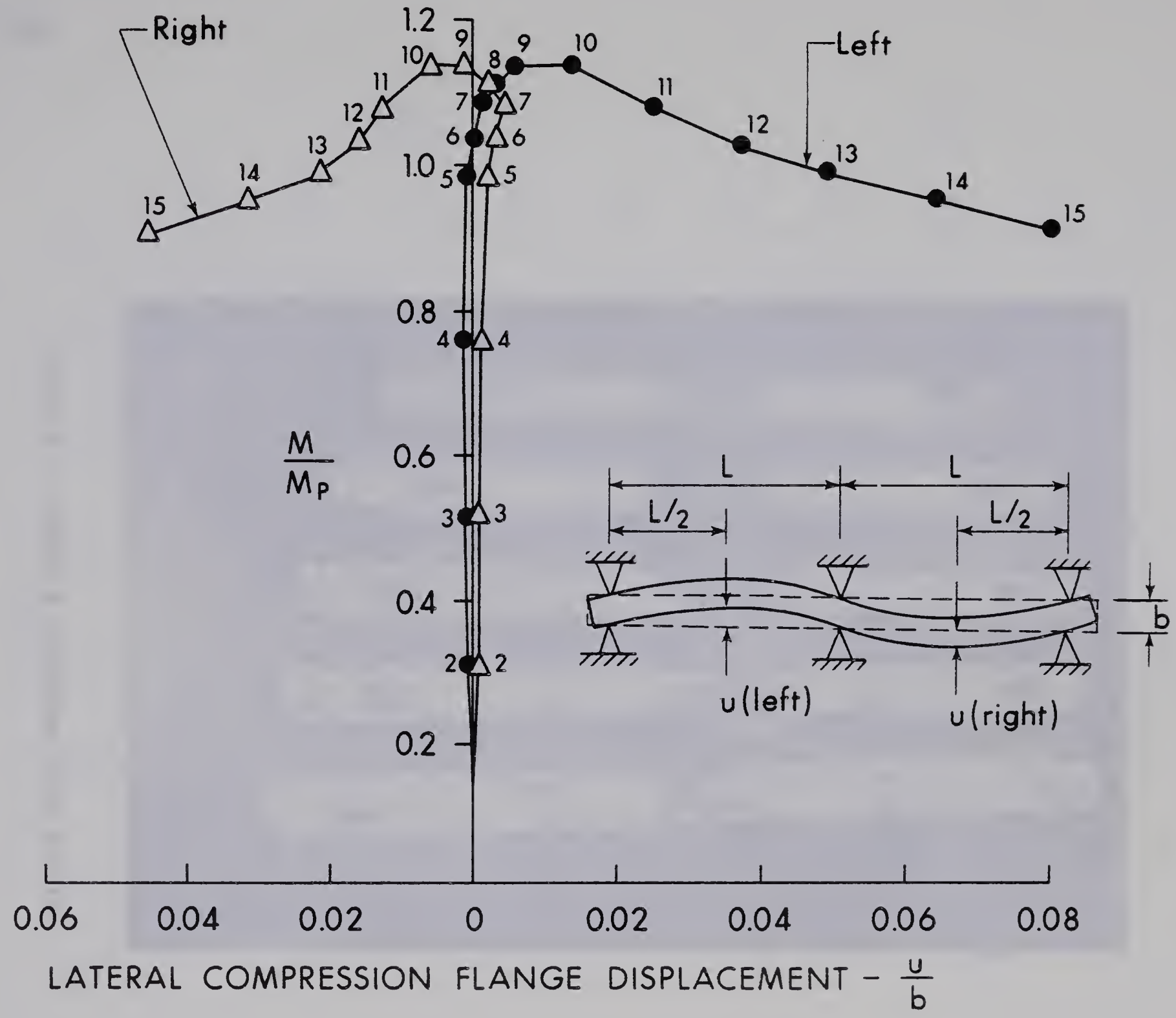

FIGURE 4.5 LATERAL DEFLECTIONS - BEAM B-3

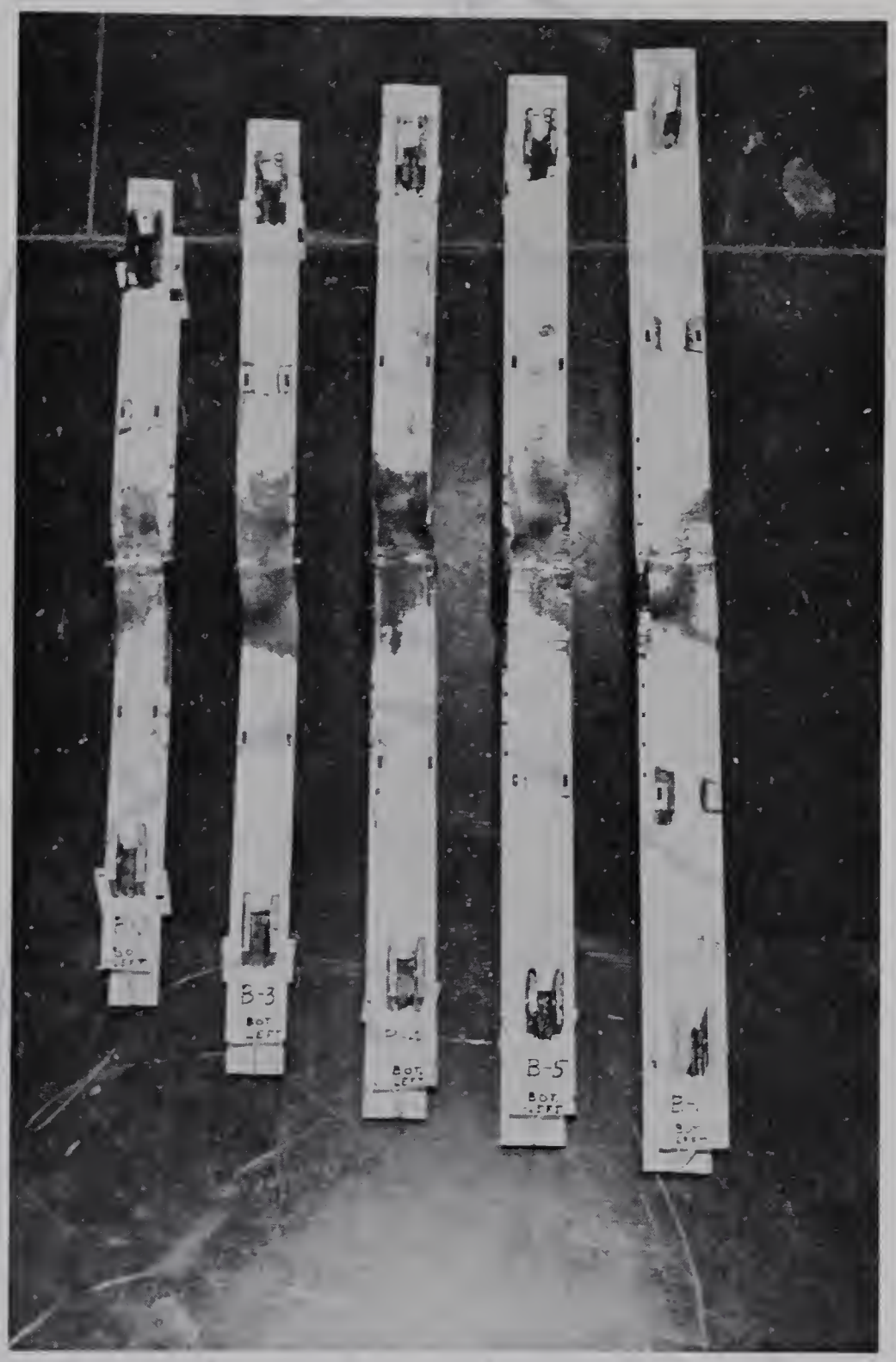

FIGURE 4.6 SERIES B SPECIMENS AFTER TESTING

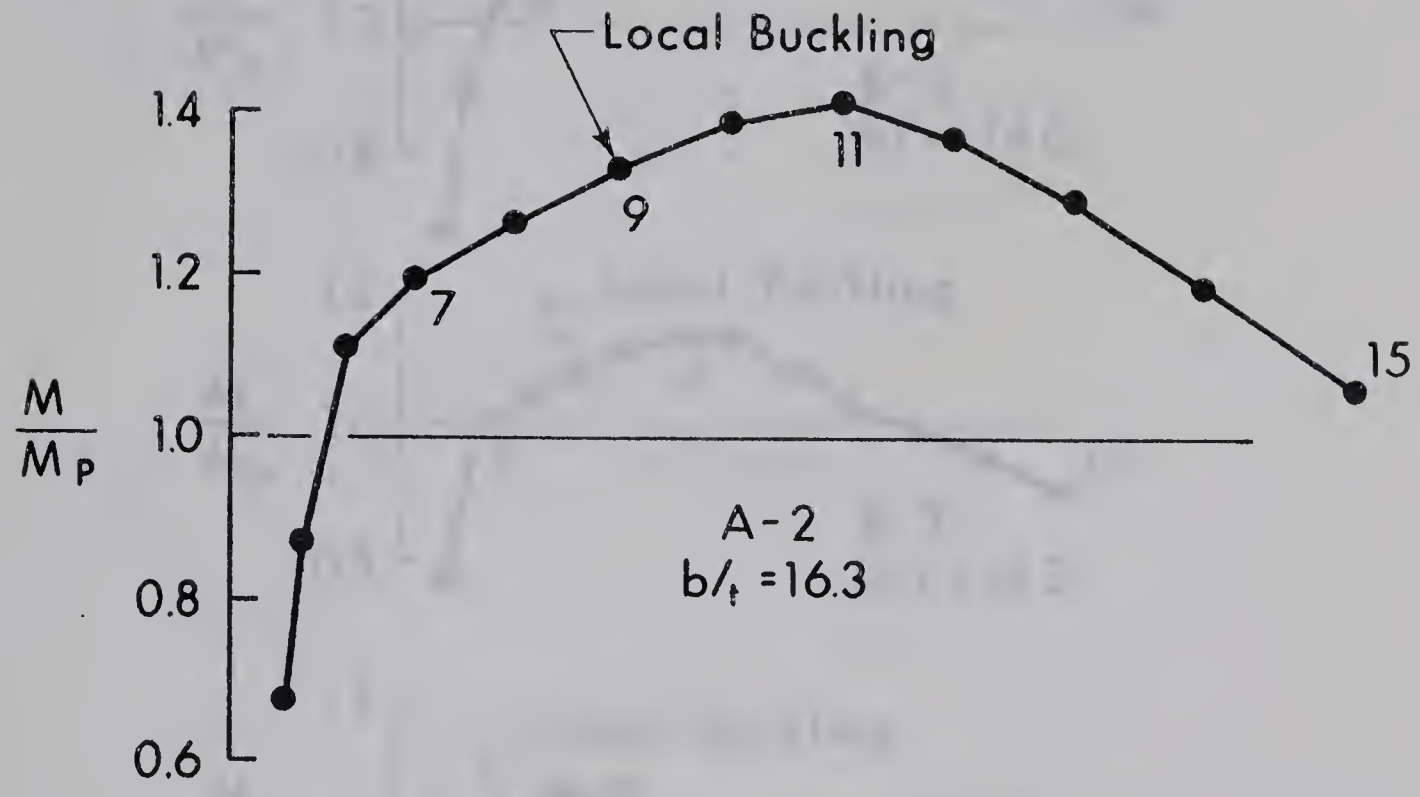

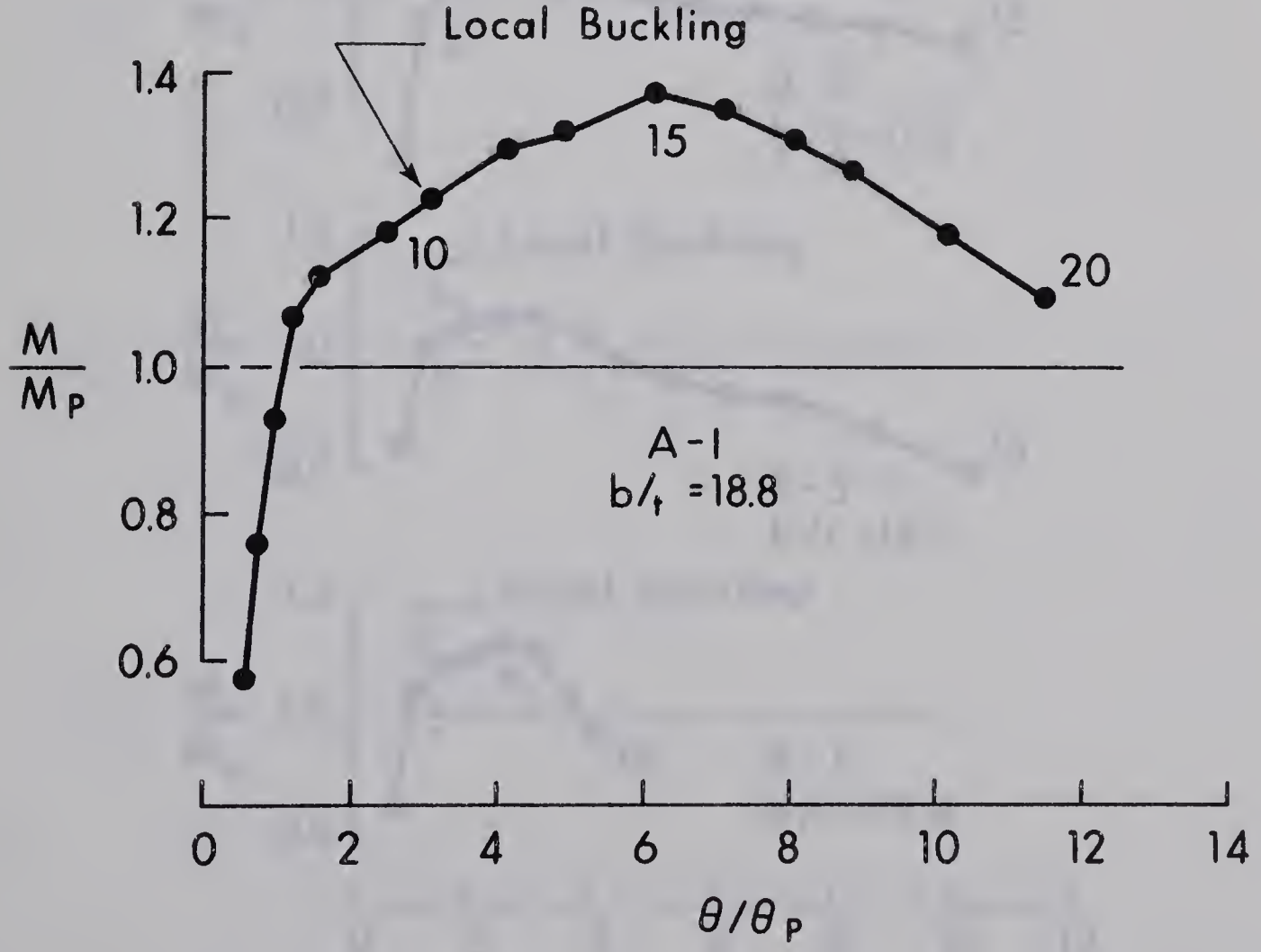

FIGURE 4.7 SERIES A MOMENT-ROTATION RELATIONSHIPS

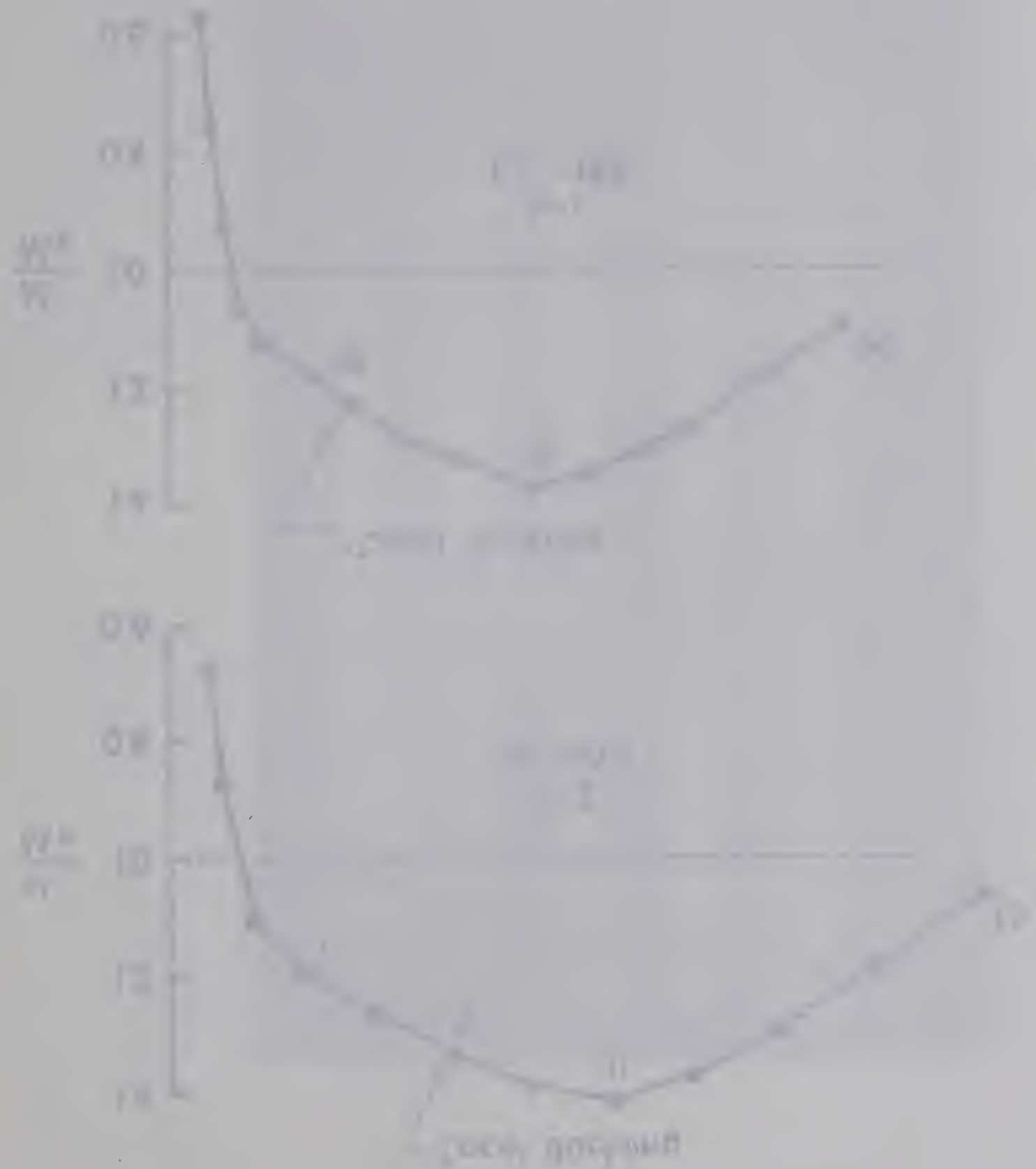

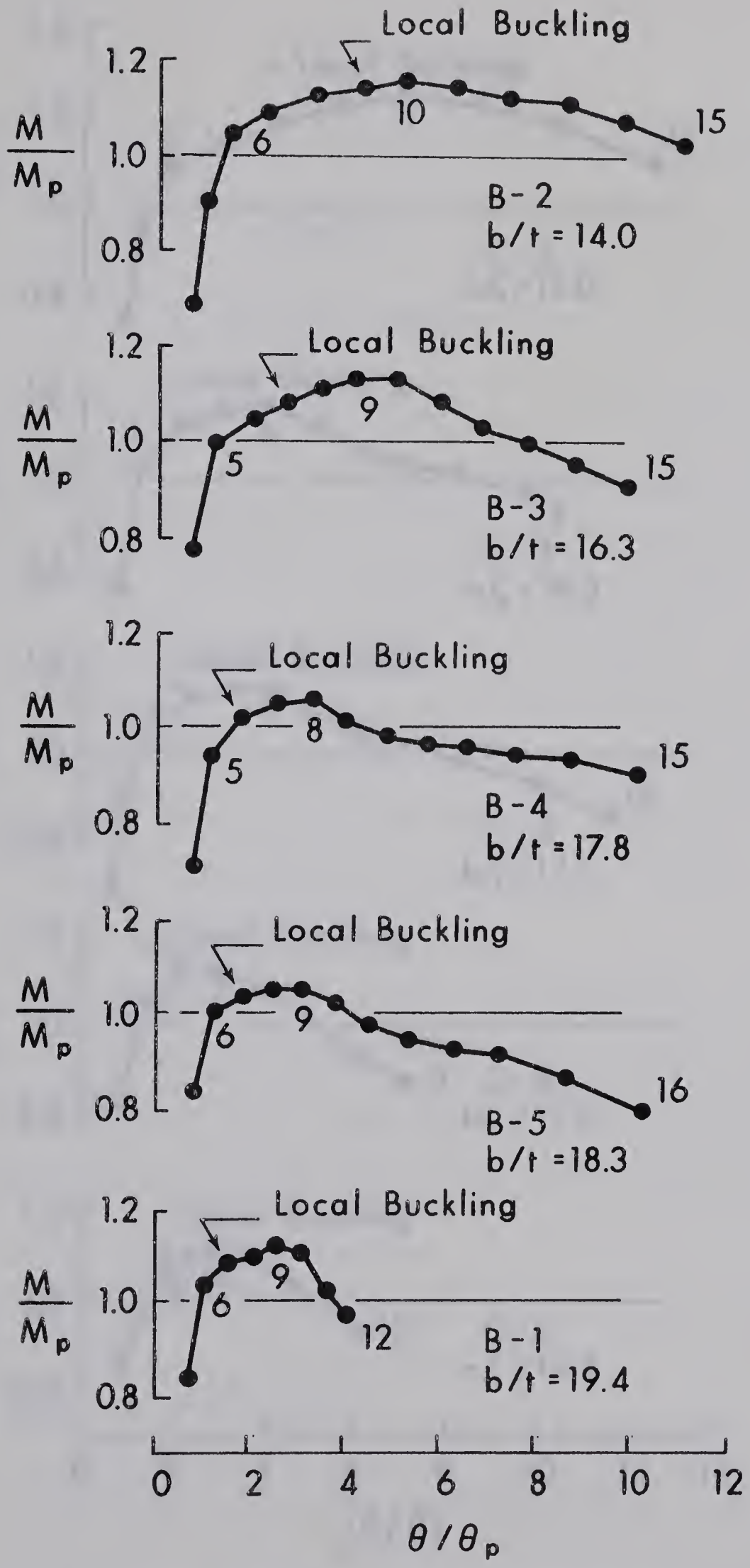

FIGURE 4.8 SERIES B MOMENT-ROTATION RELATIONSHIPS

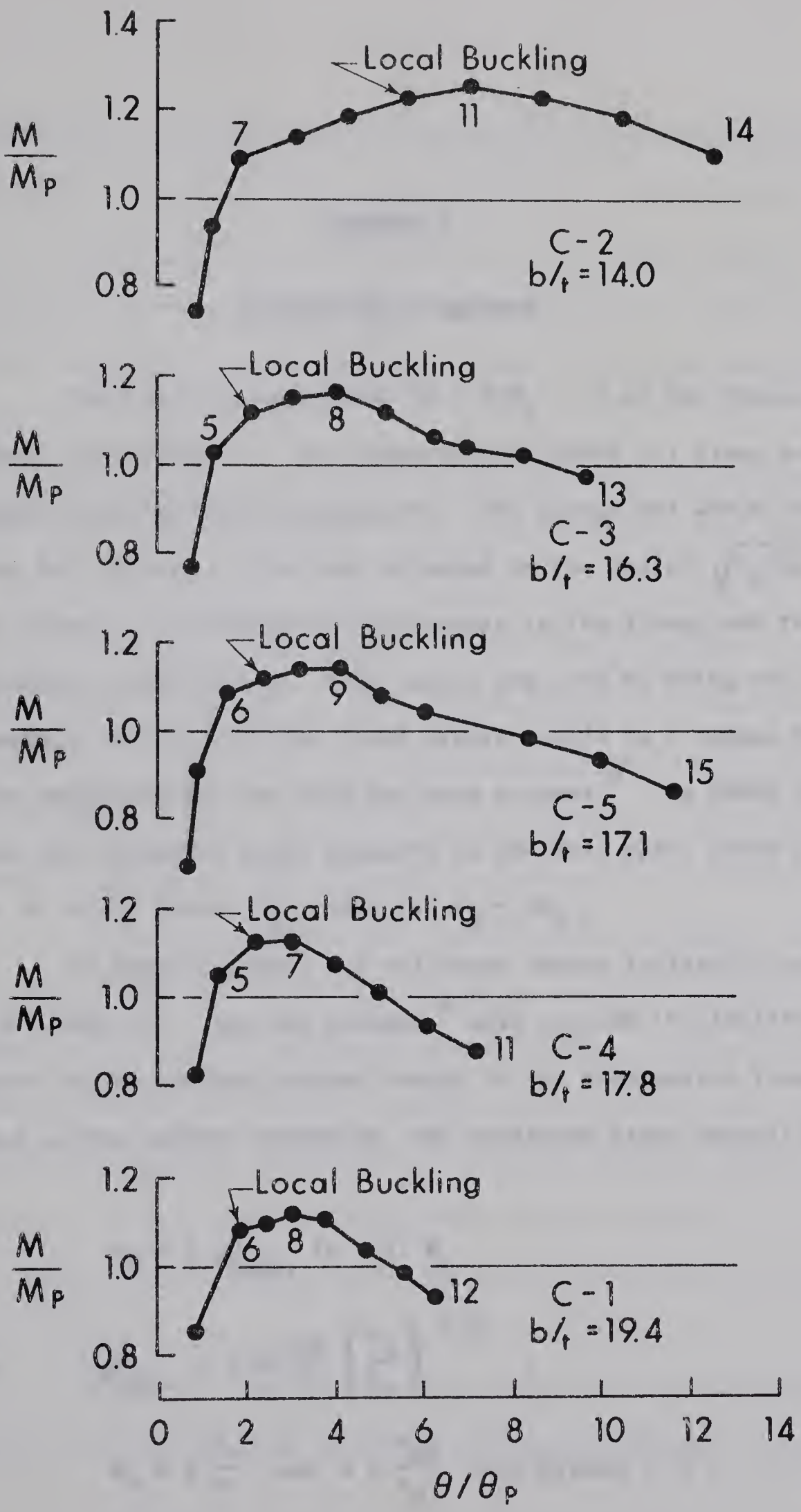

FIGURE 4.9 SERIES C MOMENT-ROTATION RELATIONSHIPS

CHAPTER V

DISCUSSION OF RESULTS

The rotation capacities ($R = \theta/\theta_p - 1$) of the Series A beams, obtained from FIGURE 4.7, are summarized in TABLE 5.1 along with the pertinent cross-sectional properties. The flange and web slenderness ratios, b/t and d/w , have been adjusted by the factor $\sqrt{\sigma_y/44}$, where σ_y is taken as the measured yield stress in the flange and the web of the specimen respectively. This factor was used to bring the results for members having different yield stress levels to a common basis. A similar approach has been used for beam columns[22]. In TABLE 5.1, θ_H denotes the inelastic hinge capacity in the full span, taken at the point where M drops below M_p ; that is, $\theta_H = R\theta_p$.

As expected, Beam A-2 delivered larger inelastic rotations than did Beam A-1. Lay and Galambos[8] have related the inelastic hinge capacity to the optimum yielded length of the compression flange, $\ell_{opt.}$. Applied to the present situation, the predicted hinge capacity becomes:

$$\theta_T = 2\,\ell_{opt.}\,(s - 1)\,\phi_y \tag{5.1}$$

where
$$\ell_{opt.} = 1.42\,\frac{bt}{w}\left(\frac{A_w}{A_f}\right)^{1/4}, \tag{5.2}$$

$$\phi_y = 2\,\frac{\epsilon_y}{d} \quad \text{and} \quad s = \frac{\epsilon_{st}}{\epsilon_y} \quad \text{(see Figure 1.1)}$$

The development of Equation (5.1) implies that the moment capacity drops below M_p at the onset of local buckling, and that local buckling will occur when the yielded length, τL, reaches $\ell_{opt.}$. The development is strictly valid, within the assumptions used, only for sections having b/t ratios exactly equal to those given by Equation (2.5).

The predicted inelastic hinge capacity has been compared to that measured experimentally at the peak of the M-θ curve[8]. In TABLE 5.2, the values of $\ell_{opt.}$, $\tau_u L$ and ℓ_u are given. The actual length of local buckle, ℓ_u, was measured at the peak of the M-θ curve. The yielded length, $\tau_u L$, at the peak of the M-θ curve, was determined by measuring the average length over which the whitewash had spalled off the compression flange. In TABLE 5.2 θ_u denotes the experimentally-determined inelastic hinge rotations at the peak of the M-θ curve.

For both tests in Series A, the yielded lengths, $\tau_u L$, were approximately equal to the values of $\ell_{opt.}$, but the measured wavelengths, ℓ_u, were only about one-half of $\ell_{opt.}$ Local buckling was initiated, however, at yielded lengths considerably below $\tau_u L$. The experimental inelastic rotations were approximately twice those predicted by theory. If the total useful inelastic hinge capacity, θ_H (TABLE 5.1), rather than θ_u is compared with θ_T, the predictions are grossly conservative.

TABLES 5.3 and 5.4 present the information obtained from the Series B and C tests. For the beams in these series the rotation capacities,

R , and the hinge capacities, Θ_H , decreased significantly as the flange slenderness increased.

A comparison of the test results with the predictions given by Lay and Galambos[8] shows some interesting trends. The measured wavelengths of the local buckles, ℓ_u , are approximately equal to the yielded lengths, $\tau_u L$. This would indicate that the buckled lengths were restricted by the relatively small extent of yielding due to the high moment gradients in the Series B and C tests. This restriction would also be predicted by the theory, since the yielded lengths, $\tau_u L$, are much smaller than the computed optimum wavelengths, $\ell_{opt.}$.

The relationship between τL and $\ell_{opt.}$ will also affect the correlation between the measured hinge rotations, Θ_u , and the predicted rotations, Θ_T . Therefore, the predicted values should be reduced to compensate for the high moment gradients[5.1]. If $V_{opt.}$ is defined as the moment gradient corresponding to $\tau L = \ell_{opt.}$, and V_u is the moment gradient on the member at the peak of the M-Θ curve, then the adjusted values of Θ_T would be: $\bar{\Theta}_T = \Theta_T V_{opt.}/V_u$. This development assumes that the maximum moment value for a given beam is dependent only on the section and material properties, and is constant for all values of moment gradient greater than $V_{opt.}$.

In TABLE 5.5 the ratio $V_{opt.}/V_u$ is listed for all tests, along with the adjusted prediction of the hinge rotation, $\bar{\Theta}_T$. FIGURE 5.1 summarizes the data by plotting the ratio of experimental to predicted rotations, $\Theta_u/\bar{\Theta}_T$, versus the flange slenderness ratio $b/t\sqrt{\sigma_y/44}$.

The tests of Series B and C plot as a fairly narrow band. These were tests in which the length of the local buckle was restricted by the high moment gradient ($V_{opt.}/V_u$ less than 1.0). On the other hand, the Series A tests plot well above the others. For these tests, V_u was less than $V_{opt.}$, so that the buckled wavelength was not restricted by the extent of yielding.

Thus, it appears that the inelastic hinge rotations of beams having small moment gradients are not necessarily limited by the attainment of an optimum yielded length of the compression flange.

The trend of higher inelastic hinge rotations for members subjected to lower moment gradients is again evident if the total hinge capacity, θ_H is used as a basis of comparison. FIGURE 5.2 plots the values of $\bar{\theta}_H = \theta_H \; V_u/V_{opt.}$ against $b/t\sqrt{\sigma_y/44}$. The factor $V_u/V_{opt.}$ is applied to account for the restriction of buckled lengths due to high moment gradients. Although its application to the unloading range of the M-θ curve has no theoretical significance, a study of the test curves shows this to be not unreasonable. The trend in FIGURE 5.2 is similar to that in FIGURE 5.1.

The above conclusions are partially confirmed by a group of tests performed on A441 steel beams under moment gradient[6]. Three tests were performed in this series, two in which the lengths of the local buckles were restricted by the high moment gradient, and one in which the optimum length was fully yielded. The pertinent results of these three tests are summarized in TABLE 5.6 and plotted in FIGURES

5.1 and 5.2 as open circles. The total hinge capacity, θ_H , for Test HT-52 is considerably above those for the two companion beams. The values of θ_u , however, are approximately the same for the three tests.

One additional series of tests has been performed on beams under moment gradient[10]. The results of these tests have been discussed and compared with predicted values[8]. They showed the same trends with respect to beams under low moment gradients as discussed herein.

Test	$\frac{b}{t}\sqrt{\frac{\sigma y}{44}}$	$\frac{d}{w}\sqrt{\frac{\sigma y}{44}}$	R	θ_H (Radians)
A-1	18.25	33.1	11.8	0.260
A-2	15.80	33.1	13.6	0.272

TABLE 5.1 SERIES A - TOTAL ROTATIONS

Test	$\tau_u L$ (in.)	$\ell_{opt.}$ (in.)	ℓ_u (in.)	θ_u (Radians)	θ_T (Radians)
A-1	13.35	15.5	8.35	0.1134	0.0674
A-2	13.00	14.0	7.6	0.1220	0.0603

TABLE 5.2 SERIES A - YIELDED LENGTHS AND PEAK ROTATIONS

Test	$\frac{b}{t}\sqrt{\frac{\sigma y}{44}}$	$\frac{d}{w}\sqrt{\frac{\sigma y}{44}}$	R	θ_H (Radians)
B-1	21.5	51.6	2.9	0.042
B-2	15.5	51.6	10.4	0.120
B-3	18.07	51.6	6.7	0.092
B-4	19.73	51.6	3.4	0.052
B-5	20.3	51.6	3.2	0.048
C-1	21.5	58.6	4.2	0.049
C-2	15.5	58.6	13.7	0.112
C-3	18.07	58.6	8.0	0.078
C-4	19.73	58.6	4.2	0.045
C-5	18.95	58.6	6.5	0.068

TABLE 5.3 SERIES B AND C - TOTAL ROTATIONS

Test	$\tau_u L$ (in.)	$\ell_{opt.}$ (in.)	ℓ_u (in.)	θ_u (Radians)	θ_T (Radians)
B-1	3.1	7.70	3.5	0.0282	0.0982
B-2	3.8	6.03	3.0	0.0488	0.0767
B-3	4.1	6.76	3.1	0.0518	0.0863
B-4	3.8	7.22	3.5	0.0302	0.0920
B-5	3.25	7.37	3.1	0.0296	0.0940
C-1	4.5	7.90	3.3	0.0236	0.0650
C-2	4.3	6.18	2.7	0.0483	0.0510
C-3	3.65	6.94	3.5	0.0296	0.0572
C-4	3.8	7.40	3.5	0.0216	0.0610
C-5	4.3	7.16	4.6	0.0316	0.0593

TABLE 5.4 SERIES B AND C - YIELDED LENGTHS AND PEAK ROTATIONS

Test	$\frac{V_{opt.}}{V_u} \leq 1.0$	$\bar{\theta}_T = \theta_T \frac{V_{opt.}}{V_u}$ Radians	$\frac{\theta_u}{\bar{\theta}_T}$	$\bar{\theta}_H = \theta_H \frac{V_u}{V_{opt.}}$ Radians
A-1	1.0	0.0674	1.69	0.260
A-2	1.0	0.0603	2.02	0.272
B-1	0.746	0.0733	0.40	0.056
B-2	0.595	0.0455	1.07	0.202
B-3	0.633	0.0545	0.95	0.145
B-4	0.741	0.0682	0.44	0.070
B-5	0.757	0.0711	0.42	0.063
C-1	0.770	0.0500	0.47	0.064
C-2	0.606	0.0309	1.56	0.185
C-3	0.710	0.0405	0.73	0.110
C-4	0.764	0.0464	0.47	0.059
C-5	0.747	0.0442	0.72	0.091

TABLE 5.5 PRESENT TESTS - ADJUSTED ROTATIONS

Test	$\frac{b}{t}\sqrt{\frac{\sigma y}{44}}$	θ_u (Radians)	$\frac{V_{opt.}}{V_u}$	θ_T (Radians)	$\bar{\theta}_T$ (Radians)	$\frac{\theta_u}{\bar{\theta}_T}$	θ_H (Radians)	$\bar{\theta}_H$ (Radians)
HT-43	18.2	0.039	0.56	0.105	0.059	0.66	0.060	0.107
HT-28	18.2	0.074	0.85	0.105	0.088	0.84	0.104	0.124
HT-52	18.2	0.086	1.0	0.105	0.105	0.82	0.200*	0.200

*Extrapolated from Published Curves

TABLE 5.6 LEHIGH UNIVERSITY TESTS

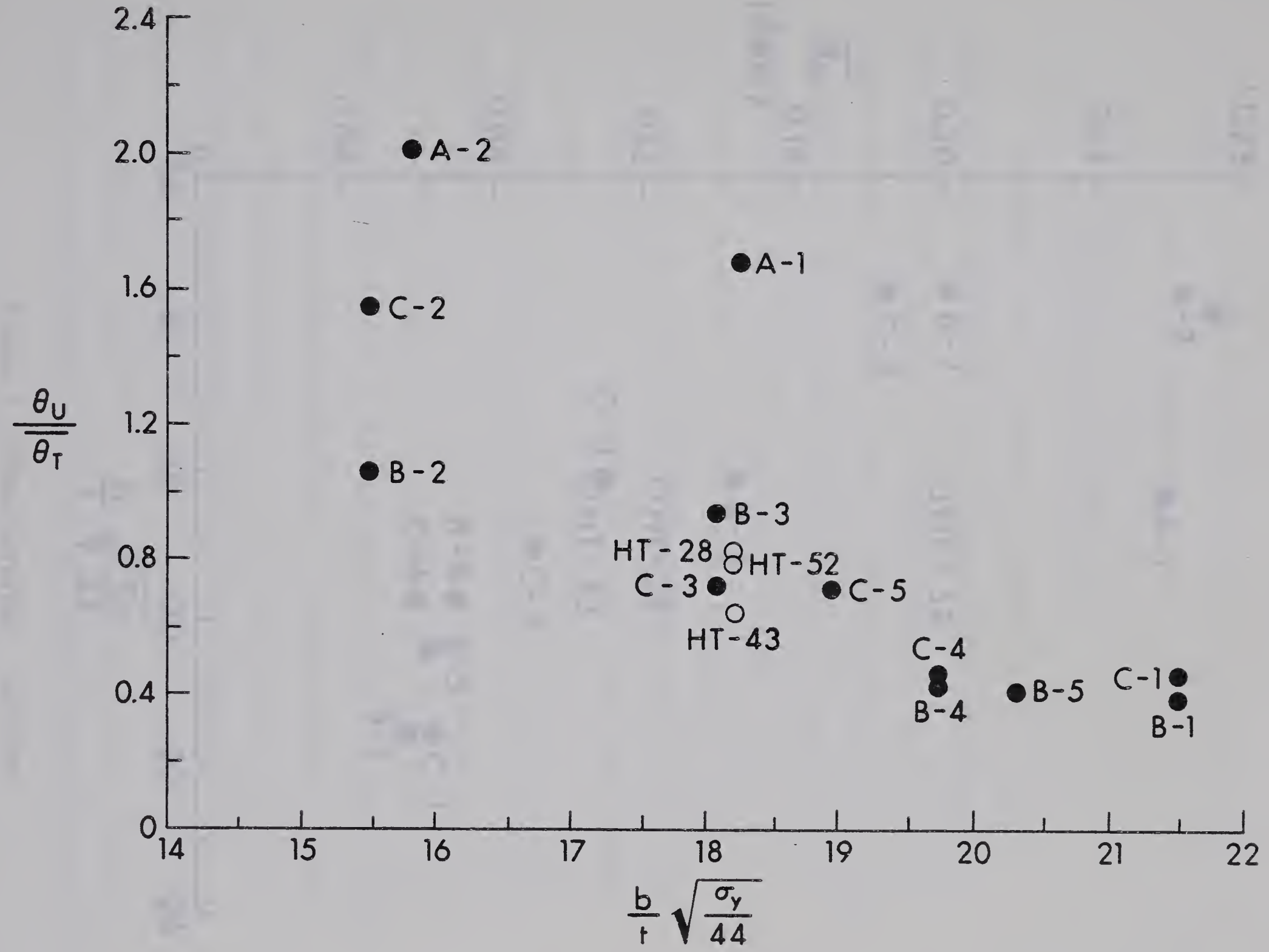

FIGURE 5.1 PEAK ROTATIONS - EXPERIMENTAL/THEORETICAL

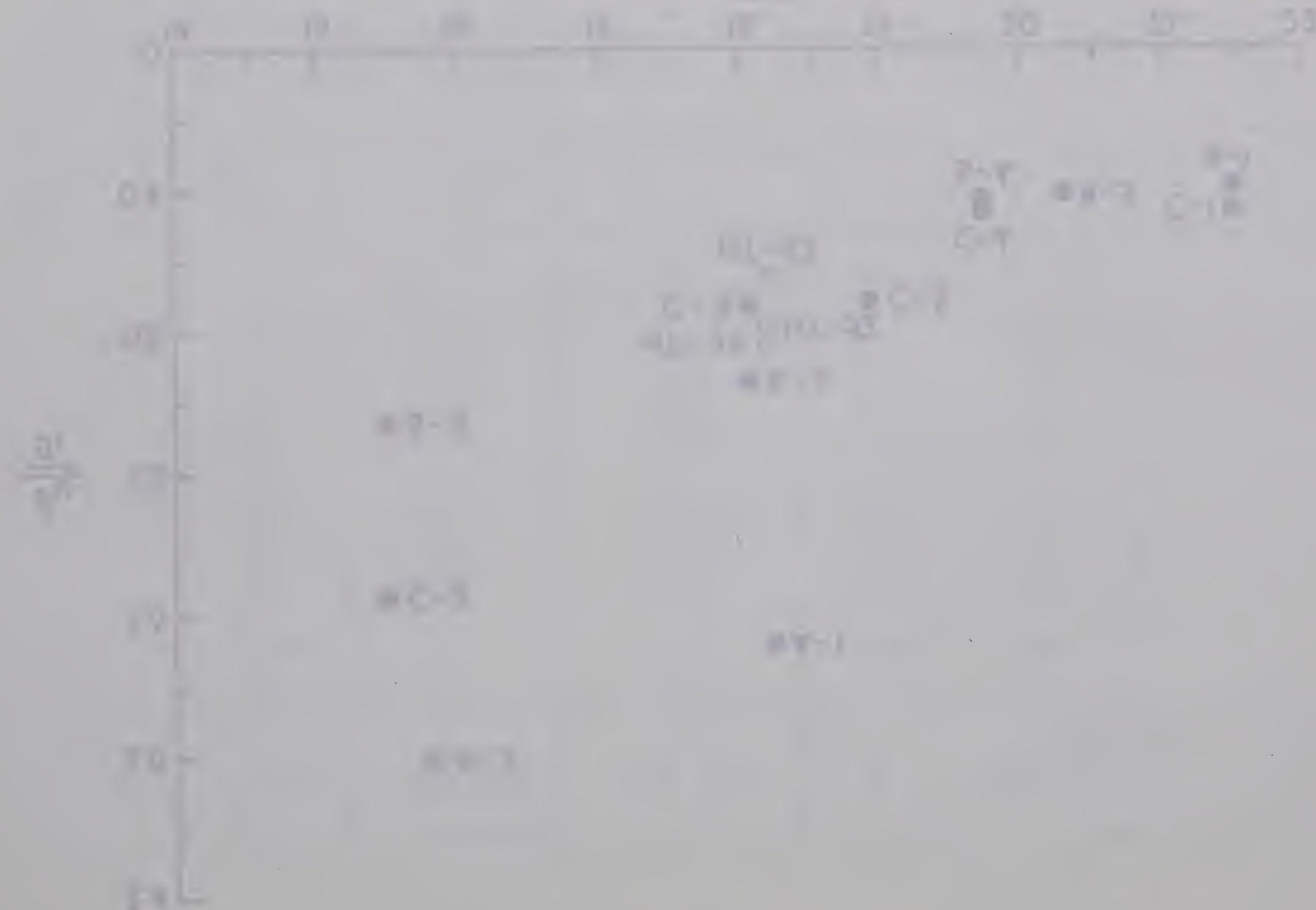

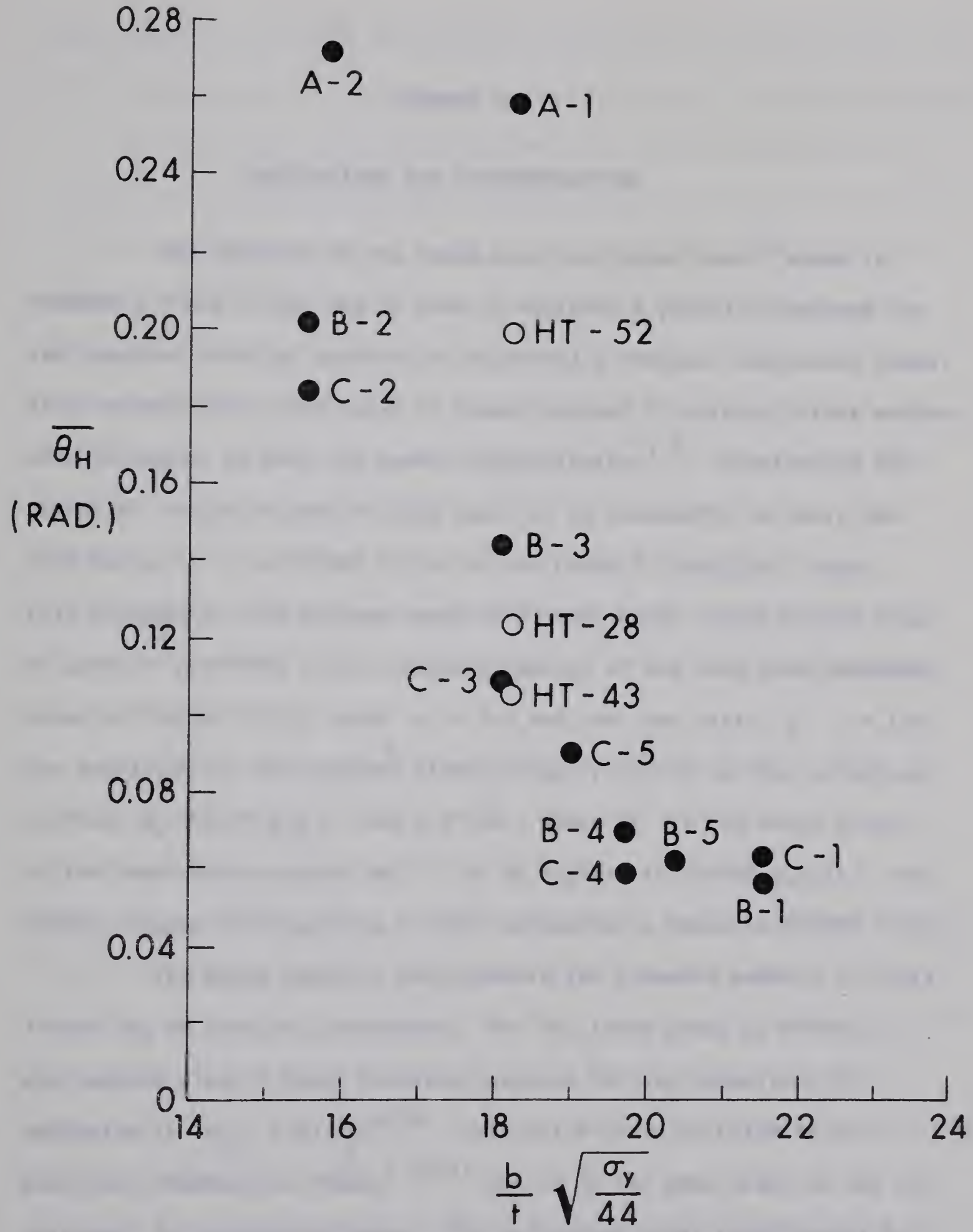

FIGURE 5.2 TOTAL ROTATIONS - ADJUSTED

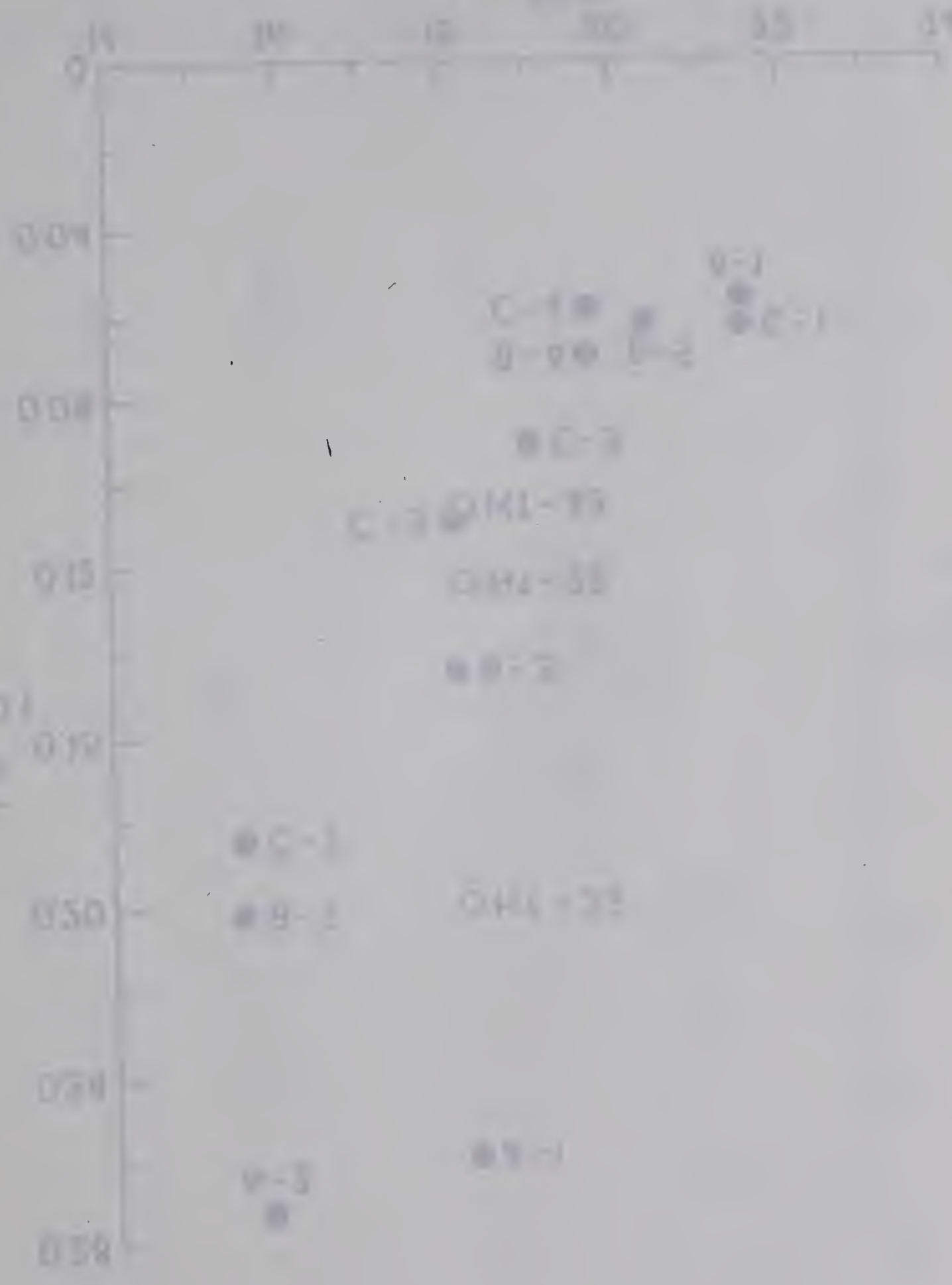

CHAPTER VI

CONCLUSIONS AND RECOMMENDATIONS

The analysis of the three-span continuous beam[15] shown in FIGURES 2.7 and 6.1(a) can be used to estimate a practical maximum for the required rotation capacity of plastically designed continuous beams. This estimate will also apply to beams designed by working stress methods when allowance is made for moment redistribution[1,2]. Considering the practical ratios of dead to live load, it is reasonable to limit the load ratio, β , in FIGURE 6.1(a) to the range $0.33\alpha \leq \beta \leq 3.0$. Under this assumption, the maximum required plastic hinge rotation will occur at point B in FIGURE 6.1(a) during formation of the side span mechanism shown in FIGURE 6.1(b), with β = 3.0 and the span ratio, α , = 1.0. The magnitude of the required plastic hinge rotation in this situation is then, $\theta_R = 0.83\ \phi_p L = 1.66\ \epsilon_y f\ L/d$, where f is the shape factor of the beam cross-section and L is as defined in FIGURE 6.1(a). The moment diagram corresponding to this mechanism is shown in FIGURE 6.1(c).

The hinge capacity requirements for flexural members in rigid frames can be similarly estimated. For the frame shown in FIGURE 2.8 the maximum plastic hinge rotation required for the formation of a mechanism is $\theta_R = 1.03\ \phi_p L$[4,16]. This value could be taken as the practical maximum for frames[4,16,17] and is of the same order as the requirement for continuous beams. The calculated hinge requirements for

both frames[16] and beams[15] were based on simple plastic theory, which has been shown by a more exact analysis to overestimate the true requirements[23].

The hinge rotation requirement for a continuous beam can be related to the experimental hinge capacity of a particular test specimen. This can be accomplished by determining the continuous beam span which is equivalent to that of the test specimen, and then calculating the hinge rotation required in this equivalent continuous beam. For beams in which the wavelength of the local buckle is restricted by the extent of yielding (as in the case of the Series B and C tests) the available hinge rotation can be considered to be inversely proportional to the moment gradient[8]. Thus, by comparing the moment diagram given in FIGURE 6.1(c) with that for the present test beams, it is evident that the equivalent span of the continuous beam is approximately 4/5 L (for $\alpha = 1.0$).

In the case of Beam B-1, which has a value of L/d = 7.78, the equivalent value of L/d will be 4/5 x 7.78 = 6.22. The plastic rotation requirement for Test B-1 is, therefore, $\theta_R = 1.66\ \epsilon_y f\ L/d = 0.021$ radian ($\epsilon_y = 0.00183$ and $f = 1.14$). This value is only half the delivered hinge capacity, $\theta_H = 0.042$ radian, for Beam B-1. Since this specimen had the lowest ratio of hinge capacity to L/d of any tested, it is concluded that hinge rotation requirements for short beams, such as the ones in this series, can be easily met, even by the most slender-flanged specimens tested ($b/t\sqrt{\sigma_y/44} = 21.5$).

The largest hinge rotations, however, are required for very

long members. Because of limitations on allowable working load deflections, it can be reasonably assumed that the span to depth ratio, L/d , would not exceed a value of 40 for wide-flange beams having a yield stress of 44 ksi. Assuming L/d = 40 , σ_y = 44 ksi and f = 1.15, the required hinge rotation is θ_R = 0.113 radian[15] . For a higher strength steel, ϵ_y would be increased in proportion to σ_y , which would tend to increase θ_R . However, the same span deflection limitation would be imposed for both steels. Thus, the value of L/d permitted would be reduced in inverse proportion to σ_y , so that the net effect would be to leave θ_R unchanged (= 0.113 radian).

In order to relate this requirement to the results of the present test series, it is necessary to extrapolate the test results to beams of much greater lengths. One approach to this would be to use the values of $\bar{\theta}_H$ plotted in FIGURE 5.2. The calculation of these values was based essentially on the assumption that the hinge capacity is limited strictly by the attainment of the optimum yielded length of the compression flange[8]. This assumption also implies that $\bar{\theta}_H$ must be reduced when applied to the unsymmetrical moment gradient case represented by FIGURE 6.1(c), because the compression flange would then buckle to the right of load point, B , before the yielded length to the left of the load had reached $\ell_{opt.}$. However, the extrapolated hinge capacities given in FIGURE 5.2 plot considerably below the hinge capacities obtained from the tests on longer beams. This indicates that the foregoing assumption is not generally valid, and is overly-conservative

when used to predict long-beam hinge capacities from short-beam test results. Acceptance of these values would result in rather stringent b/t requirements for long beams.

A more accurate prediction would have to account for the fact that local buckling does not necessarily occur at the attainment of a yielded length = $\ell_{opt.}$. It may occur at values of the yielded length either greater or smaller than $\ell_{opt.}$, depending primarily on the stress level in the yielded zone and the properties of the cross-section, as well as on other factors.

No attempt will be made here to formulate a theory incorporating these factors. In any event, such a theory would have to be verified experimentally by tests on beams under low moment gradients. Since sufficient data of this nature is not available, it is concluded that the most urgent need at present is for additional tests on beams subjected to low moment gradients.

In addition, more tests are required to define the effects of the lateral bracing spacing on hinge capacity. In such tests it would be desirable to use an arrangement in which the moment gradient and the unbraced span could be varied independently. Such has not been the case in the present test series and others[6,10] and this has resulted in some difficulty in interpreting the results.

TABLE 6.1 lists a proposed series of 12 tests which would provide additional required information regarding the effects of varying moment gradient, flange slenderness, and lateral bracing spacing

on the hinge capacities of wide-flange beams. The range of flange slenderness included is from $b/t\sqrt{\sigma_y/44} = 16.5$ to $b/t\sqrt{\sigma_y/44} = 21.0$. From the presently available information, it appears probable that practical beams under moment gradient would deliver sufficient hinge capacity if their b/t values were near the middle of this range.

Eight of the proposed tests are on beams subjected to relatively low moment gradients ($V_{opt.}/V_u = 1.5$ to 2.5). These tests, in conjunction with the companion tests on beams with a high moment gradient, should sufficiently define the effect on the hinge capacity of lowering the moment gradient. Thus, as well as providing direct information on long beams, they would facilitate the more accurate extrapolation of previous short-beam test results.

The proposed lateral slenderness ratios cover a range of L/r_y from 35 up to 100, which is much greater than present code limitations[1,2]. The intermediate value of 60 is close to the present CSA code limitation[1] for beams of G40.12 steel[18]. Available tests on beams under moment gradient[6] have shown very little reduction in rotation capacity for beams having values of L/r_y up to 72; therefore, the tests have been proposed to include an even wider range.

In two instances, the value of L/r_y would be held constant while the moment gradient was varied. This should provide useful information regarding the individual effects of these two parameters, which would aid in the interpretation of other test results.

The results of the proposed test series would be expected to

provide sufficient basis upon which to make specific design recommendations with respect to the limiting b/t and L/r_y values for plastically-designed beams under moment gradient. Such recommendations are not possible at present, but there is evidence to indicate that current code limitations[1,2] could be relaxed somewhat.

$\frac{b}{t}\sqrt{\frac{\sigma y}{44}}$ / $\frac{V_{opt.}}{V_u}$		16.5	18.0	19.5	21.0
0.9	$\frac{L}{r_y}$	=35	35	35	35
1.5		60	60	60	60
2.5		100	60	100	60

TABLE 6.1 PROPOSED BEAM TESTS

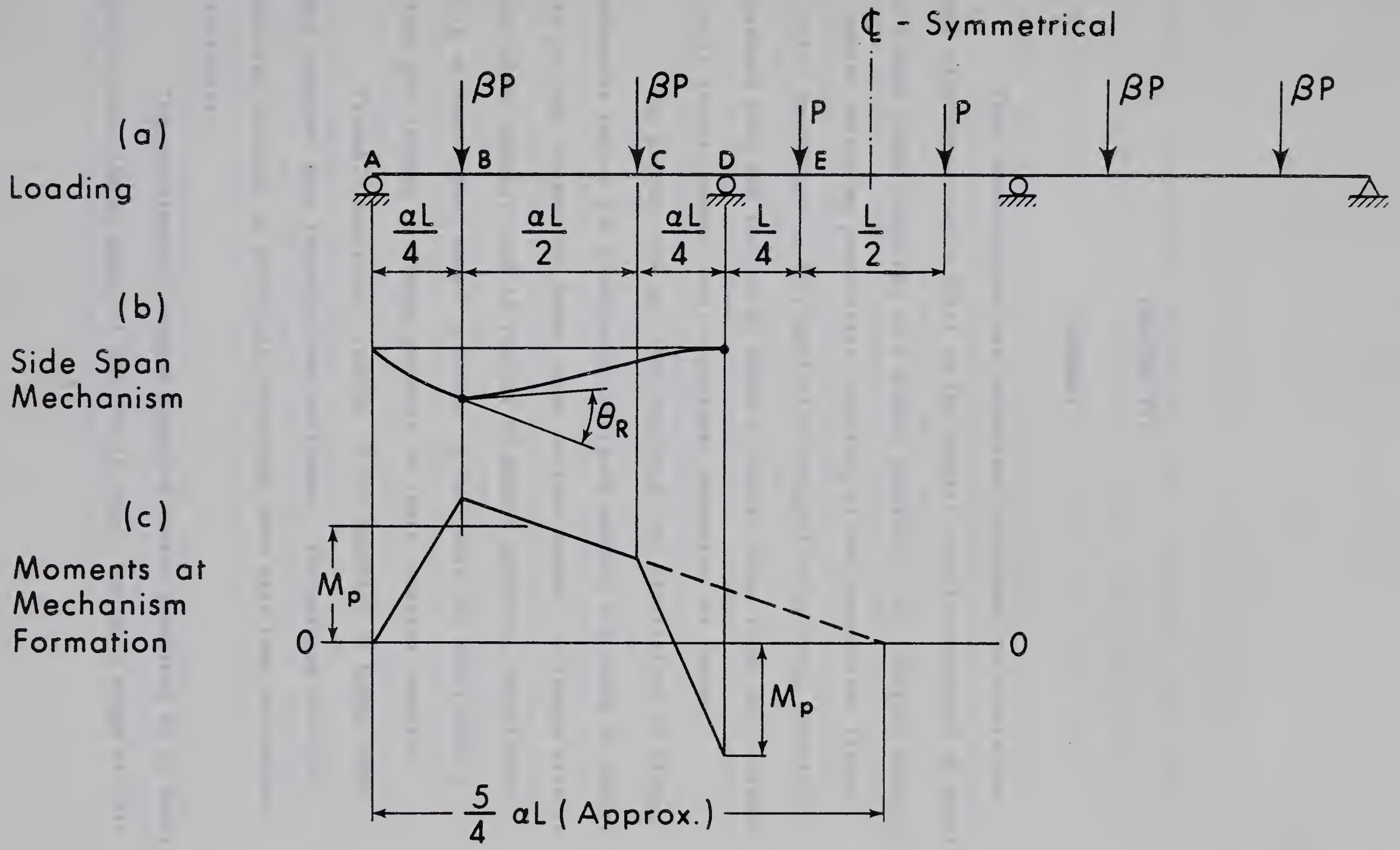

FIGURE 6.1 CONTINUOUS BEAM

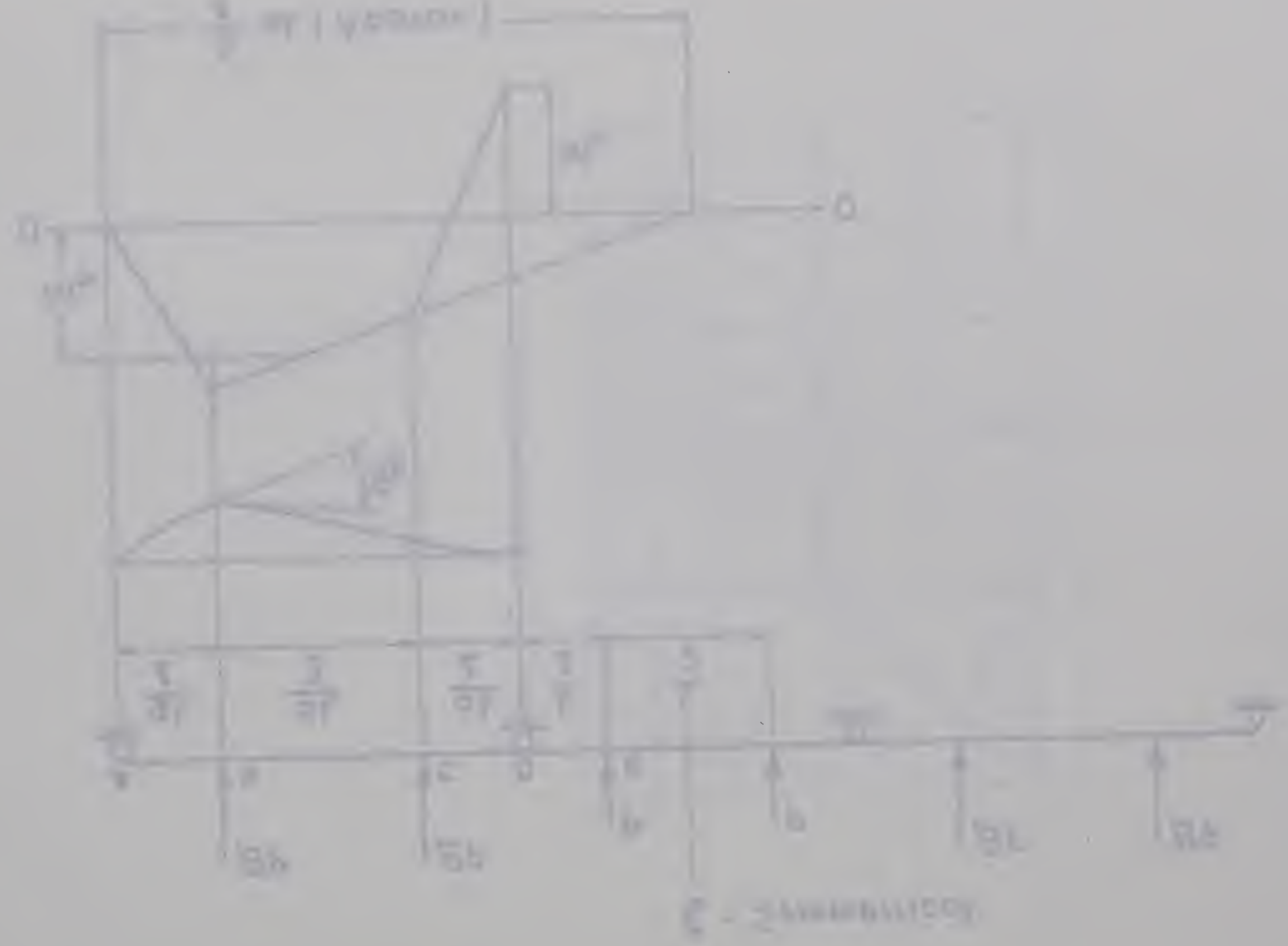

CHAPTER VII

SUMMARY

This investigation was undertaken to attempt to relate the flange slenderness ratio (b/t) to the plastic rotation capacity of steel wide-flange beams subjected to a moment gradient. The rotation capacity is limited mainly by post-elastic buckling of the compression flange. Its prime importance is in plastically designed structures, wherein it is assumed that any section at which a plastic hinge forms will sustain the full plastic moment until a collapse mechanism has formed.

The present CSA and AISC building code limitations on flange slenderness ratios for plastically designed members are based on experiments on stub columns and beams under uniform moment. Although plastic hinges most commonly form in regions of moment gradient, experimental results on beams under moment gradient to date have not sufficiently defined the effects of flange geometry on their rotation capacity.

Valuable analytical studies of the behavior of beams under moment gradient have recently been performed. The maximum rotation capacities required in practical structures have also been determined analytically.

The experimental program reported herein consisted of 12 tests on rolled wide-flange beams of CSA-G40.12 steel, having a range of b/t

values from 14.0 to 19.4. The specimens were simply supported and subjected to a concentrated load at midspan. Lateral bracing was provided at the load and reaction points, and the value of the unbraced slenderness ratio, L/r_y, was approximately 35 for all beams. All tests were continued well into the unloading range.

A wide range of rotation capacities was observed for the beams tested. As expected, the members having slender flanges delivered smaller rotation capacities than did the stockier members. Unloading was accompanied in all cases by local buckling and large lateral deformations of the unbraced span of the compression flange.

The hinge capacities delivered by the present test specimens and others were compared to the maximum requirements for practical continuous beams. For short beams, such as the test specimens, the requirements were easily met by even the most slender-flanged sections tested. The experimental short-beam hinge capacities were then extrapolated in order to relate them to long-beam rotation requirements. This extrapolation, based partially on existing theory, indicated that rather stringent b/t limitations would be needed in order to meet the large hinge capacity requirements for long beams. However, the limited available tests on longer beams showed the extrapolation to be overly conservative in each case. Since long-beam rotation requirements are the governing consideration, it was concluded that more long-beam (low moment gradient) tests are required before firm conclusions can be drawn with regard to allowable flange slenderness ratios.

A further series of tests is proposed which would include beams under relatively low moment gradients. In addition, the lateral bracing spacing would be varied (independently of the moment gradient) over a wide range, and the flange slenderness would again be varied over a suitable range. It is expected that the results of this test series, in conjunction with the presently available test results, would provide sufficient basis upon which to make specific design recommendations. These recommendations would include both the limiting flange slenderness ratio and the lateral bracing spacing for plastically designed beams under moment gradient.

NOMENCLATURE

A_f	Flange area
A_w	Web area
b	Flange width
d	Depth of section
E	Modulus of elasticity
E_{st}	Strain-hardening modulus
f	Shape factor
G	Shear modulus
G_{st}	Strain-hardening shear modulus
h	Ratio of elastic to strain-hardening modulus
I	Moment of inertia
I_w	Warping moment of inertia
K_T	St. Venant torsional constant
k_ϕ	Web spring constant
L	Length
$\ell_{opt.}$	Theoretical optimum wavelength of local buckle
ℓ_u	Measured wavelength of local buckle at maximum moment
M	Moment
M_o	Maximum moment in span
M_p	Plastic moment
M_{ps}	Moment at which flange is fully yielded

n Number of half-wavelengths of local buckle

P Load

P_u Collapse load

R Rotation capacity

r_y Weak axis radius of gyration

S Adjacent span spring constant

s Ratio of strain-hardening strain to yield strain

t Flange thickness

$V_{opt.}$ Shear force assumed to correspond to a yielded flange length of $\ell_{opt.}$

V_u Maximum attained shear force

w Thickness of web

α Length ratio

β Load ratio

ϵ Strain

ϵ_{cr} Strain at onset of local buckling

ϵ_{st} Strain at onset of strain-hardening

ϵ_y Yield strain

θ Rotation

θ_H Inelastic hinge rotation (hinge capacity)

$\bar{\theta}_H$ Maximum hinge capacity (extrapolated)

θ_R Required hinge capacity

θ_T Theoretical delivered hinge capacity

$\bar{\theta}_T$ Theoretical delivered hinge capacity adjusted for effects of high moment gradient

θ_u Delivered inelastic hinge rotation at maximum moment

λ Slenderness factor

μ Poisson's ratio

σ Stress

σ_u Ultimate stress

σ_y Yield stress

τ Proportion of flange length yielded

τ_u Proportion of flange length yielded at maximum moment

ϕ_p Curvature corresponding to M_p assuming ideally elastic material

LIST OF REFERENCES

1. CSA - "Steel Structures for Buildings", Canadian Standards Association Standard S-16, 1965.

2. AISC - "Specification for the Design, Fabrication and Erection of Structural Steel for Buildings", American Institute of Steel Construction, 1961.

3. Lay, M.G. and Galambos, T.V. - "Inelastic Steel Beams Under Uniform Moment", Proc. ASCE, Vol. 91, ST6, December 1965.

4. Lee, G.C. and Galambos, T.V. - "Post-Buckling Strength of Wide-Flange Beams", Proc. ASCE, Vol. 88, EM1, February 1962.

5. Galambos, T.V. - "Inelastic Lateral Buckling of Beams", Proc. ASCE, Vol. 89, ST5, October 1963.

6. Adams, P.F., Lay, M.G. and Galambos, T.V. - "Experiments on High Strength Steel Members", Welding Research Council Bulletin No. 110, November 1965.

7. Lay, M.G. - "Flange Local Buckling in Wide-Flange Shapes", Proc. ASCE, Vol. 91, ST6, December 1965.

8. Lay, M.G. and Galambos, T.V. - "Inelastic Beams Under Moment Gradient", Proc. ASCE, Vol. 93, ST1, February 1967.

9. Haaijer, G. and Thurlimann, B. - "Local Buckling of Wide-Flange Shapes", Lehigh University, Fritz Laboratory Report No. 205E.5, December 1954.

10. Sawyer, H.A. Jr. - "Post-Elastic Behavior of Wide-Flange Steel Beams", Proc. ASCE, Vol. 87, ST8, December 1961.

11. Bleich, F. - "Buckling Strength of Metal Structures", McGraw-Hill Book Company, Inc., New York, 1952.

12. Kato, B. - "Buckling Strength of Plates in the Plastic Range", Communication with L.S. Beedle, February 1960.

13. ASTM -"Mechanical Testing of Steel Products", American Society for Testing Materials Standard A370-65.

14. Ferrara, A. and Galambos, T.V. - Discussion of "Post-Elastic Behavior of Wide-Flange Steel Beams", Proc. ASCE, Vol. 88, ST4, August 1962.

15. Kerfoot, R.P. - "Rotation Capacity of Beams", Lehigh University, Fritz Laboratory Report No. 297.14, March 1965.

16. Driscoll, G.C. Jr. - "Rotation Capacity Requirements for Beams and Frames of Structural Steel", Ph.D. Dissertation, Lehigh University, 1958.

17. ASCE and WRC - "Commentary on Plastic Design in Steel", ASCE Manual No. 41, 1961.

18. CSA - "General Purpose Structural Steel", Canadian Standards Association Standard G40.12, 1964.

19. Adams, P.F. and Galambos, T.V. - "Material Considerations in Plastic Design", Lehigh University, Fritz Laboratory Report No. 297.23, November 1966.

20. Huber, A.W. and Beedle, L.S. - "Residual Stress and the Compressive Strength of Steel", Welding Journal, 33(12), Research Supplement 589-S to 614-S, December 1954.

21. Yarimici, E., Yura, J.A. and Lu, L.W. - "Techniques for Testing Structures Permitted to Sway", Lehigh University, Fritz Laboratory Report No. 273.40, May 1966.

22. Lu, L.W. - "Columns, Lecture Notes on Plastic Design of Multi-Story Frames", Chapter 4, Lehigh University, Fritz Laboratory Report No. 273.20, 1965.

23. Adams, P.F. - "Plastic Design in High Strength Steel", Lehigh University, Fritz Laboratory Report No. 297.19, May 1966.